Shallow fault systems of thrust anticlines responding to changes in accretionary prism lithology (Nankai, SE Japan)

Abubakar Maunde[a, b, *], Tiago M. Alves[a], Gregory F. Moore[c]

[a] 3D Seismic Laboratory, School of Earth and Environmental Sciences, Cardiff University, Main Building, Park Place, Cardiff, CF10 3AT, United Kingdom

[b] Department of Geology, School of Physical Sciences, Modibbo Adama University of Technology, P.M.B. 2076, Yola, Nigeria

[c] Department of Earth Sciences, University of Hawaii, 1680 East-West Rd., Honolulu, HI 96822, United States

***Corresponding author**: E-mail: abubakarmaunde@mautech.edu.ng; maundea@cardiff.ac.uk Telephone: +2348161358265

Abstract

Three-dimensional (3D) pre-stack depth migrated seismic data are used to analyse the geometry and growth of shallow faults associated with tectonic shortening in four (4) prominent thrust anticlines off Nankai, SE Japan. The four thrust anticlines show a trench-ward increase in horizontal shortening and deform the seafloor at present. They shortened the overburden strata by 7143 m in the Late Quaternary, reflecting a horizontal shortening of 32.9% in response to plate subduction. A significant number of closely-spaced and segmented fault arrays is observed in their hinge regions. We show that vertically segmented fault arrays with local throw maxima between 5 and 14 m relate to the existence of more competent (strong) intervals, or layers. Incompetent (weak) intervals where record relatively small throw values between 2 to 5 m. The observed mechanical layering is likely to continue at depth to control stress accumulation in faults posed to reactivate during seismic events. We show that the presence of closely-spaced, segmented fault arrays at shallow stratigraphic levels can have a significant impact on local stress distribution, controlling near-seafloor strain in accretionary prisms as Nankai's.

Keywords: Subduction zones; Nankai Trough; Tectonic shortening; Mechanical stratigraphy; Fault growth; Segment linkage.

1. Introduction

Offshore SE Japan, the subduction of the Philippine Sea Plate beneath the southeast margin of Eurasia occurs at a variable convergence rate of 4.0 to 6.5 cm/year (e.g., Seno et al., 1993; Miyazaki and Heki, 2001; DeMets et al., 2010). This process has led, since the Pliocene-Pleistocene, to large-scale tectonic shortening and uplift of overburden strata above a subducted oceanic slab to form the Nankai accretionary prism, i.e. a mass of sediment that has been scrapped off from the subducting Philippine Sea Plate and accreted together with sediment derived from SE Japan (e.g., Taira, 2001; Miyazaki and Heki, 2001; Bird, 2003; Kimura et al., 2011, 2018). The continuous movement of the subducted Philippine Sea Plate has induced a

continuum of internal deformation that is expressed in the form of imbricate thrust faults, thrust anticlines, pop-up structures, megasplay faults, strike-slip faults, and dip-slip faults (e.g., Kimura et al., 2011; Moore et al., 2013; Alves et al., 2013; Lin et al. 2015; Van Tuyl et al., 2015; Azevêdo et al., 2018).

Several studies have shown how local stress fields can control faulting and accretionary prism deformation in Nankai (e.g., Wu et al., 2013; Moore et al., 2013; Van Tuyl et al., 2015; Lin et al. 2015; Chang and Song, 2016). For instance, Moore et al. (2013) and Van Tuyl et al. (2015) suggested that stress decoupling occurs between a shallow regime of extensional normal faulting and a deeper regime of strike-slip faulting and thrusting in both the inner and outer wedge regions of the Nankai accretionary prism. Authors such as Chang and Song (2016) have recently postulated that structures in the inner wedge region of Nankai reflect strike-slip and normal faulting stress regimes as horizontal and vertical stresses show similar magnitudes. In fact, strike-slip and extensional structures are found in both core and regional seismic data from the inner wedge of Nankai. In the outer wedge region, Azevêdo et al. (2018) and Lackey et al. (2020) showed that strike-slip, together with thrusting, are the two major styles of deformation. The outer wedge region of the Nankai accretionary prism thus comprises closely spaced, synthetic forethrusts, antithetic backthrusts and corresponding anticlines that occur, near the seafloor, in association with shallow fault systems.

Despite the growing number of studies addressing the relationship between local stress and SE Japan's structural evolution, the published literature has thus far overlooked the effect of mechanical stratigraphy on fault geometry and growth off Nankai, in great part due to the relative lack of borehole data acquired in its outer wedge region. This results in a relative underrepresentation of the true structural evolution of the Nankai Trough as a whole; outcrop and seismic data in other regions of the world often relate the styles and geometries of faults with mechanical-stratigraphic differences in the host rocks (e.g., Childs et al., 1996; Ferrill and Morris, 2003, 2008; Childs et al. 2009; Ferrill et al., 2014; Tvedt et al. 2013; Ferrill et al., 2017; Libak et al., 2019). This is an important caveat, the relationship between faulting and mechanical stratigraphy can be used either to predict fault style and geometry or, conversely, interpret mechanical stratigraphy based on characterisation of the fault styles and geometries (Ferrill and Morris, 2003, 2008; Ferrill et al., 2017).

This article explores a set of shallow fault systems from areas dominated by thrust anticlines in the outer wedge region of the Nankai accretionary prism (SE Japan), aiming to address the following questions:

a) What are the geometries and styles of shallow fault populations in areas dominated by tectonic shortening such as the Nankai accretionary prism?

b) What mode(s) of fault propagation and growth are observed in the successions blanketing the outer wedge region of Nankai?

c) Can the geometry and distribution of shallow fault populations in the uppermost strata of the Nankai accretionary prism provide information about the mechanical stratigraphy of strata in this region?

In this work, we use the terms incompetent (weak) and competent (strong) to describe the mechanical stratigraphy. Incompetent (weak) intervals, or layers, are ductile and can accommodate greater amounts of prefailure strain than competent (strong) intervals under the same conditions. The latter (stronger) intervals tend to resist deformation and accommodate little deformation before brittle failure (Ferrill and Morris, 2008; Ferrill et al., 2017). Moreover, incompetent intervals can act as detachments that cause decoupling and prevent propagation of faults across specific intervals, resulting in a preferable horizontal propagation of faults to the detriment of their vertical growth (e.g., Pascoe et al., 1999; Bahroudi et al., 2003; Withjack and Callaway 2000; Richardson et al., 2005; Gabrielsen et al., 2016).

2. Geological setting

2.1. Subduction-related plates in Nankai

The study area spans the boundary between the Eurasian and the Amurian Plates, being limited to the east by the Pacific Plate and to the south by the Philippine Sea Plate (e.g., Bird, 2003; Kimura et al., 2011, 2018) (Fig. 1a). The Philippines, Pacific, and Amurian Plates converge under the Tokyo metropolitan area, resulting in a uniquely complex tectonic environment; the Amurian Plate overrides the Philippine Sea Plate, at the same time the Pacific Plate dips beneath both the Philippine Sea and Amurian Plates (e.g., Bird, 2003; Kimura et al., 2011) (Fig. 1a). These convergent plate margins generate large earthquakes within and in between the latter tectonic plates, e.g. the 1944 Tonankai and 1946 Nankai earthquake events along the Nankai Trough, and the 1923 Great Kanto Earthquake along the Sagami Trough (e.g., Harris, 1998; Ide et al., 2011; Lee et al., 2011).

Three major subduction-related boundaries, marked by deep-ocean trenches or troughs, define the tectonic setting of Nankai: a) the Sagami Trough at the interface of the Philippine Sea and Amurian Plates, b) the Japan Trench between the Amurian and Pacific plates, and c) the Nankai Trough between the Philippine Sea and the Eurasian Plates (e.g., Bird, 2003; Kimura et al., 2011) (Fig. 1a). The Nankai Trough, comprising the oceanward boundary of the study area, delineates an active (and seismogenic) convergent margin under which the Philippine Sea Plate is subducted at a variable convergence rate of approximately 4.0–6.5 cm/year, following an azimuth of 300^{o} to 315^{o} (e.g., Seno et al., 1993; Miyazaki and Heki, 2001; DeMets et al., 2010; Moore et al., 2013; Tsiju et al., 2014) (Fig. 1a, b).

The relatively shallow nature of the Nankai Trough results in part from fast subduction of young Shikoku Basin crust, which deforms the thick sediment cover of the subducting plate (Moore et al., 2015). This sediment-dominated subduction zone has led to the accumulation of a relatively thick accretionary prism, several hundred kilometers wide, that is limited to the northwest by the Kumano (forearc) Basin and to the southeast by the Shikoku Basin (e.g., Kinoshita et al., 2010; Kopf et al., 2010) (Fig. 1b).

2.2. Structural styles of the Nankai accretionary prism

The deformation styles of accretionary prisms have been explained via the Coulomb and dynamic coulomb-wedge theories (e.g., Davis et al., 1983; Dahlen, 1984; Wang and Hu, 2006). These two theories propose a transition between a highly compressional outer wedge and a less compressional (and moderately seismogenic) inner wedge. As a result, Wang and Hu (2006) described the outer wedge region of the Nankai accretionary prism as comprising a series of imbricate thrust faults reflecting the low shear strength of materials, while the inner wedge region forms a zone of accreted sediment characterised by the absence of active compressional structures, thus normally acting as a backstop.

More recently, Wu et al. (2013) and Lin et al. (2015) used a compilation of borehole and core data to determine stress states and deformational styles across the Nankai accretionary prism. The authors showed that, in its inner wedge (Kumano Basin), maximum horizontal stresses (H_{Max}) have been responsible for significant strike-slip faulting. However, sediment in this same Kumano Basin records a vertical direction to the maximum stress, a configuration that reflects a normal faulting regime. This led to the conclusion that the Nankai accretionary prism is currently experiencing a predominantly (inter-seismic) extensional regime (Wu et al., 2013; Lin et al., 2015).

Lin et al. (2015) and Lackey et al. (2020) also showed evidence for compression seawards from a so-called Megasplay Fault Zone, with a maximum principal stress parallel to the convergence vector. They stated that, at present, the Nankai accretionary prism is dominated by a shallow extensional regime and a relatively deep strike-slip to reverse faulting regime, mainly due to stress field reorganisation in the areas where maximum principal stress becomes horizontal. This transition zone between different tectonic regimes is often referred to as the Extension-Compression Depth (e.g., Lewis et al., 2013; Van Tuyl et al., 2015; Lin et al., 2015).

Azevêdo et al. (2018) interpreted seismic data in the outer wedge region of the Nankai accretionary prism to reveal a set of thrusts, pop-up structures, thrust anticlines and strike-slip faults hinting at a complex strain distribution across SE Japan. The authors suggest that lateral slip, together with thrusting and folding, are the major styles of deformation operating in the outer wedge region of the Nankai accretionary prism. Both styles of deformation reflect a transpressional tectonic regime under which the maximum horizontal stress is geometrically close to the convergence vector.

3. Data and methods

3.1. Seismic data

Three-dimensional (3D) pre-stack depth migrated seismic data were used in this study. The data were acquired in the outer wedge region of the Nankai accretionary prism, SE Japan, between 33.0°-33.2°N and 136.5°-136.8°E (Fig. 1b). The survey area is oriented at N150° and covers an area of approximately 12 km by 23 km in water depths ranging between 2500 m and 5000 m. The seismic data was acquired using dual airguns and an array of four 4500 m-long streamers with a spacing of 150 m. This configuration provided a 30-fold coverage and a maximum lateral resolution of 12.5 m. Data were recorded with a 2 ms vertical sampling interval, and a 12.5 x 18.75 m bin size. After being processed, seismic data on an interpretation workstation is displayed with 5 m vertical sampling, and the minimum fault offset resolved on-

screen varies from 2 m to 6 m. The seismic data was zero-phase pre-stack depth migrated (Moore et al., 2009), and displayed with a normal positive polarity (SEG's European convention), so that an increase in acoustic impedance is represented by a red seismic reflection.

In the interpreted seismic volume, shallow faults and thrust-related anticlines are well preserved in the accretionary prism sediments (Unit II). Vertical seismic resolution approaches 6 m in shallow slope basin sediments (Unit I) based on the dominant wavelength of approximately 24 m (Alves et al., 2014). As mentioned above, fault offsets between 2 m and 6 m can be distinguished using the interpreted seismic volume. Vertical resolution in Unit II approaches 14 m based on the dominant frequency of 40 Hz and velocity of 2200 m/s. Fault offsets of 2-6 m can be recognised at this level. The overall quality of the seismic dataset is good; however, some of the reflections are weak in the deepest parts of Unit II, where complex thrust fault planes occur.

3.2. Seismic interpretation

Shallow faults and associated thrust anticlines were identified and mapped using Schlumberger's Petrel®. The seafloor horizon was mapped throughout the 3D seismic volume. From the seafloor structural map and seismic sections, we identified four (4) major thrust anticlines (A to D). In addition, we mapped three (3) horizons (H1 to H3) across the thrust anticlines to quantify any variations in the spatial and temporal horizontal shortening of these same anticlines.

We interpreted faults occurring at a stratigraphic depth interval between 20 and 1000 metres below the sea floor (mbsf) and assessed their vertical growth style through the collection of fault throws along their strikes. The measured throw values were plotted against depth to assess their nucleation points, and vertical growth styles, as well as gather information about the competence of sediments they had affected. Throw-depth (T-Z) profiles offer information on the rock competence, nucleation, growth, segmentation, and linkage of individual faults (e.g., Baudon and Cartwright, 2008; Maunde and Alves, 2020). Discrepancies in throw gradients commonly result from mechanical heterogeneities, fault reactivation and fault segmentation (e.g., Childs et al., 1996; Baudon and Cartwright, 2008; Laubach et al., 2009).

3.3. Shortening and strain measurements

Horizontal shortening (Sh) and strain (e) experienced by accretionary prism strata were measured by line-length balancing (Dahlstrom, 1969) on a series of dip line sections spaced approximately 500 m along the strike of Thrust Anticlines A to D. Horizontal shortening was measured by summing the length of the folded and faulted horizon (Lo) between the section pinpoints, minus the present-day bed length (Lf) between the same pinpoints (Fig. 2). It is worth noting, however, that the absolute value of shortening depends on the depth of reference chosen for the measurement, which may change along the length of the thrust anticlines. The strain values associated with the horizontal shortening were also computed using Equation 1.

$$e = (Lf - Lo)/Lo \quad (1)$$

where (e) is the strain, (Lf) is the present-day bed length after deformation, and (Lo) is the initial bed length before deformation (Fig. 2).

Strain (e) measurements were completed for the four (4) seismic horizons mapped in this work through the thrust anticlines (A to D). These measured strain values were plotted against distance, i.e. strain-distance (e-x) plots, as routinely used for extensional fault systems, e.g. throw-distance (T-x) plot (e.g., Baudon and Cartwright, 2008; Maunde and Alves, 2020). From the measured strain, cumulative strain and shortening for the mapped horizons through Thrust Anticlines A to D could be computed. The seismic signal is often weak in the vicinity of thrust faults, creating uncertainty in the location of fault plane and, hence, in the position of horizon cut-offs. In the Nankai seismic data, a single fault plane was usually interpreted in such regions by positioning it mid-way through the region of poor data quality. Mapped seismic horizons were extrapolated to intersect the fault plane.

Errors are associated with the digitisation of the horizon upon which shortening, and strain are measured, either by slightly increasing or decreasing the bed length, affect the calculated strain and shortening across the observed thrust anticlines. Uncertainty associated with the measurement of fault-throw values may arise from the vertical sampling rate. The sampling interval, rather than the vertical stratigraphic resolution, determines accuracy when matching two correlative seismic reflection peaks or troughs (Baudon and Cartwright, 2008). Uncertainties associated with the measurement of fault-throw values may arise either by slightly increasing or decreasing the position in depth of the recorded displacements. Errors associated with spurious velocity estimates may also affect the throw values when converted to meters. These limitations will affect the absolute value of estimated thrust anticlines shortening and fault displacements. However, the approach used in this work to quantify the variations in thrust anticlines shortening and fault displacements is robust considering the resolution of the seismic dataset.

4. Interpreted seismic units

The Nankai accretionary prism consists of slope basin sediments, accreted and underplated trench-fill turbidite facies transported axially along the Nankai Trough as a result of subduction of the Shikoku Basin crust during the Pliocene-Pleistocene (e.g., Kinoshita et al., 2010; Kopf et al., 2010). We interpreted two (2) seismic units that comprises of slope basin sediments (Unit I) and accretionary prism sediments (Unit II; Fig. 4).

4.1. Unit I: Slope basin sediments

Unit I comprise fine-grained turbidites dated as latest Pliocene to Recent and deposited in slope aprons (Kimura et al., 2011; Alves et al., 2014) (Fig. 4). The unit is discontinuous in the outer wedge of the Nankai accretionary prism, being bathymetrically confined by thrust anticlines (Fig. 4b). In seismic data, it forms a package of high frequency, continuous and moderate- to high-amplitude reflections accumulated above an angular unconformity that separates it from the underlying Unit II. This latter unit comprises strata belonging to the upper part of the accretionary prism (Kimura et al., 2011) (Fig. 4b). Three sub-units including Units Ia, Ib and Ic are recognised in the study area (Fig. 4ciii).

Silty mud and turbidites with multiple ash layers comprise the first of the sub-units, Unit Ia (Kimura et al., 2011). They are imaged in seismic data as successions of continuous high-amplitude reflections (Fig. 4ciii). The base of Unit Ia coincides with a relatively thick mass-transport deposit (MTD 6) at IODP Site C0018A (Fig. 4cii). Unit Ib comprises coarse turbidite and ash layers with interbedded silty mud and mud (e.g., Expedition 333 Scientists, 2012; Kimura et al., 2011; Strasser et al., 2012; Alves et al., 2014). It comprises a succession of low-amplitude reflections of poor to moderate continuity in seismic data (Fig. 4ciii). Lastly, Unit Ic consists of greenish/grey silty clay with beds of sand, sandy silt, silt, and volcanic ash layers (Kimura et al., 2011; Strasser et al., 2012). On seismic data, Unit Ic comprises a low- to moderate-amplitude packaged (Fig. 4ciii).

4.2. Unit II: Accretionary prism sediments

Unit II forms the upper part of the accretionary prism (Fig. 4b). It comprises thrusted hemipelagic mudstones and sands interbedded with volcanic ash and tuffs (Expedition 316 Scientists, 2009; Park et al., 2010). The unit is imaged as an interval of discontinuous and moderate-amplitude reflections, showing moderate to low frequency, that are highly deformed by thrusts and folding (Figs. 4b). The upper part of Unit II comprises high-velocity overthrusted sediments (e.g., Unit A of Park et al., 2010), while the lower part comprises of low-velocity sediments deposited above underthrusted marine sediments (e.g., Unit B of Park et al., 2010).

5. Geometry and shortening of thrust anticlines

5.1. Geometry of thrust anticlines

Seismic imaging shows that the outer wedge region of the Nankai accretionary prism is characterised by its closely spaced, NW dipping synthetic forethrusts, SE dipping antithetic backthrusts and SE-verging thrust anticlines with a linear NE-SW trend (Figs. 3 and 4b). The latter thrust anticlines were formed orthogonally to the regional bathymetric slope (Figs. 3 and 5). On the seafloor structural map in Figs. 3 and 5, these thrust anticlines can be traced along strike, having well-developed bathymetric expression, an evidence for their active growth at present. Thrust anticlines have a relatively simple bathymetric expression on the sea floor, but more complex thrusting occurs at depth (Fig. 4). The crests of the anticlines are moderately spaced and separated by 3.2 - 5.5 km, in which the synclinal basins (i.e. synclines located between the anticline crests) contain up to 350 m of growth strata with significant thinning and onlap onto the crest of the anticlines. Four major thrust anticlines (A to B) were investigated in the study area (Figs. 3, 4 and 5).

5.1.1. Thrust Anticline A

Thrust Anticline A is the most landward of thrusts in the study area. Compared to Thrust Anticlines B to D, it comprises a much broader, longer wavelength anticline, with a moderate displacement, curved forethrust on the front limb and in the anticline core (Figs. 4b and 6). Thrust Anticline A forms the landward boundary of the outer wedge region of Nankai, near the Megasplay Fault Zone (Figs. 3, 4b and 5). The thrust anticline is presently covered by slope-basin sediments (Unit I; Figs. 4b and 6), and does not have a bathymetric expression, compared to Thrust Anticlines B to D (Figs. 3, 4b and 5).

5.1.2. Thrust Anticline B

Thrust Anticline B extends outside the study area towards the southwest (Figs. 3 and 5). It is linear in plan view and formed above a seaward-verging forethrust. The forethrust terminates upwards, with some segments forming seafloor scarps (Figs. 3, 4b and 5). An antithetic backthrust, which intersects the forethrust, deforms the back limb of the anticline and dies out near the seafloor (Figs. 4b and 7). Thrust Anticline B can be traced for at least 10 km along strike on the seafloor, developing a bathymetric high with up to 102 m in relief, thus revealing active growth (Figs. 5 and 7). The thrust anticline is at least 1.4 km wide and forms a linear NE-SW trend perpendicular to the bathymetric slope (Figs. 3 and 5).

5.1.3. Thrust Anticline C

Thrust Anticline C can be traced for at least 6.0 km along strike, is 1.1 km wide, and creates bathymetric relief of up to 113 m (Figs. 3, 5 and 8). It consists of two closely-spaced thrusts. The seaward-verging forethrust dominates the structure. A second backthrust cuts the backlimb of the frontal thrust and dies out upwards, with no faults reaching the sea floor (Figs. 4b and 8). Thrust Anticline C is linear in plan view with a dominant NE trend that is also perpendicular to the bathymetric slope (Figs. 3 and 5).

5.1.4. Thrust Anticline D

Thrust Anticline D is the most distal of thrusts and extends outside the seismic dataset towards the northeast (Figs. 3 and 5). It forms the oceanward boundary of the outer wedge of Nankai accretionary prism i.e. the boundary of the main frontal thrust, which is at least 1.7 km wide on the seafloor (Figs. 3 and 5). Thrust anticline D is also a composite structure consisting of two closely spaced thrusts. The seaward-verging forethrust dominates the anticline. An antithetic backthrust deforms the back limb of the anticline and dies out upwards, with no faults offsetting the seafloor (Figs. 4b and 9). Thrust Anticline D can be traced for at least 6.0 km along strike, forming a bathymetric high of up to 182 m (Figs. 4, 5 and 9).

5.2. Spatial variations in anticline shortening

The along-strike variations in the shortening of thrust anticlines are illustrated with reference to the strain-distance (e-x) profiles in Fig. 10. Strain distribution in Thrust Anticlines A and C decreases towards their tips, showing a broadly bell-shaped distribution profile that reflects a key characteristic of structures that grow by lateral propagation (e.g., Jolly et al., 2016) (Fig. 10a, c). For Thrust Anticlines B and D, strain distribution extends outside of the interpreted seismic volume (Fig. 10b, d). Strain distribution in the mapped horizons increases with depth, it is higher in the older horizons and lower in the younger horizons, reflecting growth of the interpreted thrust anticlines through time (Fig. 10).

Local strain minima are observed between regions of strain maxima (Fig. 10). Such local minima in fault systems are typically interpreted as the signature of fault segment linkage (e.g., Baudon and Cartwright, 2008; Maunde and Alves, 2020). The relatively smaller strain values for Thrust Anticline B at 8.0 km along strike coincide with the position where the main thrust fault offsets the seafloor (Figs. 3 and 5). Shortening is always at a minimum at this location in

Thrust Anticline B (Fig. 10b). In addition, the strain (e) is always at a maximum around 6.0 km along strike, including at the level of the present-day seafloor (Fig. 10b).

Strain maxima and minima are not always in the same location for each mapped seismic horizon (Fig. 10). For example, strain maxima in H1 and H2 horizons correlate with strain minima at the seafloor at 1.0 km along the strike of Thrust Anticline B (Fig. 10b). Furthermore, at 3.0 km along this same thrust anticline, strain maxima in horizon H1 correlates with strain minima in horizons H2, H3 and near the seafloor. At 4.0 km, a broad strain minimum in the older horizon H1 corresponds with a strain maximum in horizons H2, H3 and at the seafloor (Fig. 10b). In Thrust Anticlines C and D, along-strike variations in strain show local strain minima between regions of strain maxima (Fig. 10c, d). This character indicates linkage between fold segments (e.g., Jolly et al., 2016).

5.3. Temporal variations in anticline shortening

Temporal variations in the shortening of thrust anticlines are illustrated with reference to the cumulative strain-distribution profiles in Fig. 11. The relatively poor seismic signal below horizon H1 makes it difficult to identify and map additional seismic horizons to precisely constrain the onset of tectonic shortening in the Nankai accretionary prism (Fig. 4). Thus, in this work we focused on calculating shortening for strata at H1 level or above, i.e. Late Quaternary in age. Based on the mapped horizons, shortening started prior to horizon H1 as revealed by the greater shortening values recorded at this level across all the thrust anticlines (see Lackey et al., 2020) (Figs. 10 and 11).

Thrust anticlines B and C record a relatively moderate cumulative shortening of 1524 m and 1902 m, generating relatively moderate bathymetric highs of 102 m and 113 m, respectively (Figs. 7, 8 and 11b, c). The most seaward Thrust Anticline D records the greatest cumulative shortening of 2478 m and developed bathymetric relief up to 182 m in height (Figs. 9 and 11d). The most landward Thrust Anticline A has shortened the seismic section by 1239 m and is presently buried by slope-basin sediments (Unit I; Figs. 4b and 6). Hence, it records the least cumulative shortening when compared with Thrust Anticlines B to D (Fig. 11). Thrust Anticline A consists of a single thrust (forethrust), so the accumulated shortening is expected to be relatively low compared to the more seaward Thrust Anticlines B to D, which generated both forethrust and backthrusts (Figs. 4b, 6, 7, 8 and 9).

The four studied thrust anticlines (A to D) have shortened the overburden strata by 7143 m during the late Quaternary, reflecting a horizontal shortening of 32.9% in response to plate subduction at Nankai. When compared with the results in Lackey et al. (2020), these values indicate that ~ 40% of the tectonic shortening accommodated in the outer accretionary prism is relatively young, postdating the already Late Quaternary Horizon H1.

6. Geometry and growth of shallow faults on thrust-anticline crests

6.1. Geometry of shallow faults

A significant part of shallow faults comprising normal to reverse faults is predominantly confined to Unit II. They are often observed in the hinge region of thrust anticlines (A to D;

Figs. 6-9). In Nankai, shallow faults following the trend of strike-slip faults have been classified as normal as they show minor throws without clear evidence for horizontal movement (e.g., Kimura et al., 2011; Azevêdo et al., 2018). However, these shallow faults can also comprise oblique-slip faults with their horizontal displacement below the horizontal resolution of the seismic data.

Shallow faults dissect the uppermost part of the accretionary wedge, between a stratigraphic interval of 20 and 1000 mbsf. They are very small features with displacement ranging between 2 m and 14 m, compared to the larger thrust faults that detach at underthrusted sediments, showing displacements larger than 450 m (Figs. 6-9). Shallow faults primarily result from bending and stretching of overburden strata in response to ongoing tectonic shortening offshore Nankai. Thus, they accommodate a significant part of the bending strain occurring during thrust-anticline development and associated seismic events (Figs. 6-9).

The seismic sections in Figs. 12-15 highlight some of the features of shallow faults in the uppermost part of the outer wedge region of Nankai accretionary prism. These faults are closely-spaced and vertically segmented, with some appear to propagate and link with other faults. Throws die out at different stratigraphic intervals, with no faults dissecting the seafloor (Figs. 12-15).

6.2. Growth of shallow fault

The growth of shallow faults in the study area was investigated using the throw distribution profiles in Figs. 12c-15c. These profiles show a typical mode of fault growth dominated by segment linkage, i.e. multiple throw maxima separated by throw minima in the throw distribution profiles. The throw profiles of these faults do not always have single positive gradients and are characterised by throw profiles resembling M-type patterns between their upper-tip points and immediate throw minima (e.g., Baudon and Cartwright, 2008).

Fault segments with local throw maxima between 5 and 14 m represent the intervals where faults nucleate first. Each of these fault segments propagated outwards until they encountered other pre-existing fault segments to link together. Linkage points in the imaged fault segments occur where local throw minima between 2 and 5 m are recorded (Figs. 12c-15c).

The fault segments revealing local throw maxima develop in more competent (strong) intervals. These fault segments drive displacement into less competent (weak) intervals where throw minimum is accommodated by ductile deformation. Thus, propagation of slip from fault segments with local throw maxima in more competent (strong) intervals into less competent (weak) intervals can result in the vertically segmented fault arrays observed in the seismic dataset and throw-depth (T-Z) profiles (Figs. 12-15). Such a character reflects fault propagating and growing by segment linkage, where by two separate fault segments with throw maxima have propagated towards each other and linked to form a larger fault (e.g., Baudon and Cartwright, 2008; Maunde and Alves, 2020).

7. Discussion

7.1 Impact of tectonic shortening offshore Nankai

Accretionary prims such as the Nankai Trough in SE Japan record large-scale tectonic shortening and uplift driven by plate subduction (e.g., DeMets et al., 2010; Tsuji et al., 2014). Previous studies have suggested predominant compressional tectonics operating on this prism (e.g., Kimura et al., 2011; Lin et al. 2015). However, complex set of thrust-related anticlines associated with segmented shallow faults are observed on seismic data across the outer wedge of the Nankai, hinting at a complex strain distribution between a shallow regime of dip slip faulting and a deeper regime of thrusting operating in the Nankai accretionary prism (Figs. 4b, 7, 9, 12 and 13). The thrust faults form the larger structural framework that accommodates regional compression and tectonic shortening of overburden strata in response to ongoing down-dip subduction of the Shikoku Basin crust (e.g., Kimura et al., 2011; Moore et al., 2015) (Fig. 4b). Against this backdrop, the shallow faults accommodate a significant part of the bending and stretching strain occurring during the development of thrust anticlines and subsequent local stress redistribution during seismic events in the offshore Nankai (Lin et al., 2015) (Figs. 12-15).

The four studied thrust anticlines (A to D) have shortened the overburden strata by 7143 m, reflecting a horizontal shortening of 32.9% in response to the down-dip subduction occurring in Nankai. Thrust Anticlines B, C and D have recorded significant horizontal shortening of around 1524 m, 1902 m, and 2478 m respectively, and developed bathymetric relief of up to 102 m, 113 m, and 182 m in height, respectively. They deform the seafloor, proving their active growth (Figs. 4b, 5, 11b, c and d). The proximal Thrust Anticline A records the least shortening (1239 m) and is currently buried by slope basin sediments (Figs. 4b and 5). This confirms a trenchward increase in horizontal shortening in the outer wedge region Nankai accretionary prism (Fig. 11). This active trench-ward increase in horizontal shortening of thrust anticlines may be due to overall increase in deformation rate on the entire Nankai accretionary prism. In fact, Kinoshita et al. (2010) and Kopf et al. (2010) suggests an increase of deformation rate in the outer wedge region of the Nankai accretionary prism by the subduction of the Shikoku Basin crust during the Pliocene-Pleistocene. An important issue is how tectonic shortening translate to the seafloor bathymetric expression observed in the seaward Thrust Anticlines B to D (Figs. 4b and 5).

As highlighted in Equations 2 and 3 below, horizontal shortening of overburden rocks often generates vertical uplift (Hardy and Poblet, 2005). This uplift continues as the shortening progresses except for the case of a simple fault bend fold, where the fold broadens (increases in width) without generating any further vertical relief once the lowest unit in hanging-wall reaches the upper footwall flat (Poblet and Hardy, 1995). However, tectonic shortening and uplift on continental margins is frequently associated with seafloor expression and gully erosion atop active anticlines (e.g. Mountjoy et al., 2009), a process further emphasised by climatic and oceanographic phenomena (e.g., Lewis et al., 1994; Micallef and Mountjoy, 2011).

The conceptual models in Fig. 16 illustrate the relationship between structural uplift rate, sediment accumulation rate and development of seafloor bathymetric expression. In this relationship, the ratio of the amount of sediment accumulation vs. the rate of structural uplift (or shortening) determines whether a structure develops a bathymetric expression on the

seafloor (e.g., Shaw et al., 2004, 2006; Ford et al., 1997), following Equations (2) and (3) below:

$$s = \frac{sh}{tcos\emptyset} \quad (2)$$

$$u = 2sSin\emptyset \quad (3)$$

where s is the slip rate, ∅ is fault dip, horizontal shortening is sh, t is the time frame of reference and u is the uplift rate.

For instance, when the structural uplift rate is greater than the sediment accumulation rate, sediments will onlap growing structures, their bathymetric expression will be revealed (Fig. 16a). Consequently, the growing structure would be expected to affect any sediment transported downslope due to its bathymetric expression on the seafloor. Thus, downslope sediment (e.g., Unit I; Fig. 4b) will be expected to accumulate within a mini or perched basin (i.e. syncline) created by the growing structure. In the study dataset, we identified three Thrust Anticlines (B, C and D) as having a clear bathymetric expression (Figs. 4b and 5). These structures have recorded a significant shortening and developed a corresponding bathymetric relief of up to 102 m, 113 m, and 182 m in high, respectively. Thus, lie somewhere close to the conceptual model in Fig. 16a.

When the sediment accumulation rate is greater than the uplift rate of the thrust anticline, the deposited sediments will thin over the crest of the thrust anticline, thus forming overlapping geometries that will relatively smoothen the seafloor (Fig. 16b). In the study area we identified Thrust Anticline A as having a relatively smooth bathymetry. This anticline records the least shortening (1239 m) with no corresponding bathymetric expression (Figs. 4b, 5 and 6), a geometry lying close to the conceptual model in Fig. 16b. We stress that geometries of strata observed on the flanks of growing structures, as shown in the conceptual models in Fig. 16, are not often this well-defined on seismic data - both onlapping and overlapping geometries can occur on the same growing structure, as either sediment supply or uplift rates vary through time (e.g., Shaw et al., 2004; Jolly et al., 2016).

7.2. Geometry and growth of shallow faults offshore Nankai

Research has shown that, as strain accumulates in a mechanically layered sedimentary section, brittle layers will fault first whereas ductile layers accommodate greater prefailure strain prior to faulting (e.g., Ferrill and Morris, 2003, 2008; Welch et al., 2009). Thus, faults would be expected to nucleate first in more competent layers or intervals with local throw maxima (Fig. 17a) and are later linked together in incompetent/weaker layers or intervals with local throw minima (Fig. 17c). Incompetent (weak) intervals can prevent or slow propagation of faults from other layers, so that the locus of deformation can be shifted laterally across the incompetent intervals. Such a shift in fault position across an incompetent layer can result in vertical fault segmentation, whereby the fault segments can be hard or soft-linked (e.g., Bahroudi et al. 2003; Gabrielsen et al. 2016) (Fig. 17). Therefore, it is well established in the literature that the

lithology and mechanical behaviour of the host rock influence fault kinematics and their related geometries.

In the study dataset, we observe vertical fault segmentation with alternating local fault-throw maxima and minima in the interpreted throw-depth (T-Z) profiles, a character reflecting the presence of mechanical heterogeneous successions blanketing the Nankai accretionary prism. In which fault-throw maxima are related to more competent (strong) layers or intervals, and fault-throw minima are associated with less competent (weak) intervals (Figs. 12c-15c). We also observe strong evidence for vertical fault segmentation in the interpreted seismic dataset, a character indicating the presence of incompetent (weak) intervals (Figs. 12-15). Incompetent intervals can act as detachments that cause decoupling and prevent propagation of faults across specific intervals, resulting in a preferable horizontal propagation of faults to the detriment of their vertical growth (e.g., Richardson et al., 2005; Gabrielsen et al., 2016) (Figs. 12-15). In facts, IODP Site C0006 (Expedition 316 Scientists, 2009; Fig. 4ci) recognised the presence of hemipelagic mudstone to sand, mud, and silty-clay sequences interbedded with volcanic ash and tuffs in the study interval. Thus, hinting at a presence of heterogenous lithologies blanketing the Nankai accretionary prism (Fig. 4ci).

7.3 Mechanisms of formation of shallow faults off Nankai

According to data in Price and Cosgrove (1990); Lonergan et al. (1998) and Cartwright et al. (2003) shallow normal faults can be formed by a multitude of phenomena, from near-seafloor extension over growing anticlines to sudden compaction of mud-rich strata and subsequent loss of volume and fluid to form polygonal fault families. This brings to this discussion an important question: what were the mechanisms responsible for the formation of the shallow fault families imaged in Unit II, in our study area?

The interpreted data confirm the assumption that local extension occurred in Thrust Anticlines A to D above a so-called neutral surface (Price and Cosgrove, 1990; Ramsay, 1967) –a characteristic also used by Lin et al. (2015) and Wu et al. (2013) to prove that the Nankai Trough region is experiencing an intra-seismic cycle in which compression was replaced by widespread extension. Furthermore, Van Tuyl et al. (2015) showed that a clear limit exists throughout the outer wedge region between extension and compressional stresses across what was called the Extension-Compression Depth. A complementary explanation to the formation of, at least, some of the shallow faults in our study area would be sudden compaction of a mud-rich succession, with localised fluid escape through the imaged fault planes. There are aspects that seem to both corroborate and rebuke this latter interpretation, which we will consider in the paragraphs below.

In the study area, the role of sediment compaction should be considered, but features mapped do not resemble vertical gas (of water) pipes, nor any other kind of fluid flow feature. They are limited in their height, the depths in which they occur, and there are no fluid-flow features such as pockmarks on the seafloor. They clearly offset the imaged strata within the vertical resolution limits of the seismic data - which allows us to distinguish fault offsets of up to 14 m (Figs. 12c-15c).

Compaction and fluid escape should occur in a geological setting as Nankai's, but the features mapped clearly offset the adjacent strata; they are also associated with the structural bending of the Thrust Anticlines A to D (Figs. 6-9). In addition, mechanical stratigraphy is likely to evolve through time for very 'fresh', young sediments experiencing compaction and dewatering ((Xiao and Suppe, 1989; Zoback, 2007; Ferrill et al., 2012). However, Unit II is not the youngest of strata and comprises sediment that has potentially been compacted in the last few million years (Ma), and later exhumed in Thrust Anticlines A and D to form broad antiform structures. In this particular case, Thrust Anticlines A and D are not formed by the youngest (and potentially softer) of slope-basin strata; instead, they are composed of strata in Unit II that span the Early Pleistocene to Pliocene in age (Fig. 4ci).

In essence, the shallow faults (or discontinuities) imaged in the individual reflections' present clear offsets in seismic data – well within its vertical sampling limits - and comprise a combination of normal faults, bands of compaction or dilation, and ancillary faults and fractures responding to local strike slip motion. The stated vertical resolution is ~6 m, but the mapping of fault throws as those in this work depend on the vertical sampling of the seismic data. Throws were measured from the upper tip of the fault, with zero (0) throws, to the lower tip in each of the faults. Therefore, errors in measurements obey the vertical sampling rate of the seismic data (Tao and Alves, 2019) (Figs. 12-15).

8. Conclusions

Detailed seismic interpretation of shallow faults in Nankai, showing throws between 2 m and 14 m, provided us with insights into the geometry and growth of shallow faults in this area, as well as the competence of sediments blanketing an active accretionary prism. The main conclusions of this work are as follows:

a) Offshore Nankai (SE Japan), tectonic shortening and uplift of overburden strata have induced a continuum of internal deformation that is expressed in the form of structures such as forethrusts, backthrusts and corresponding anticlines that occur, near the sea floor, in association with significant distribution of the shallow fault populations in the uppermost part of the Nankai accretionary prism. The four studied Thrust Anticlines A to D confirm a trench-ward increase in horizontal shortening and have actively grown and deformed the modern seafloor. They cumulatively shortened the study area by 7143 m, representing a horizontal shortening of about 32.9% during the late Quaternary in response to the ongoing down-dip subduction of the Shikoku Basin crust in Nankai.

b) The presence of vertically segmented fault arrays dissecting the uppermost strata with local throw maxima between 5 m and 14 m relate to the existence of more competent (strong) intervals. Linkage points of these segmented fault throw maxima occur where local throw minima between 2 and 5 m are recorded in less competent (weak) intervals. Hence, multiple throw maxima separated by throw minima on the throw distribution profiles show that fault segment linkage is a common process during the growth of shallow faults in the uppermost part of the outer wedge region of Nankai accretionary prism.

c) The presence of closely-spaced and vertically segmented fault arrays observed in the seismic dataset confirm the existence of incompetent (weak) lithologies. Incompetent (weak) lithologies, or layers, can act as local detachments that cause stress decoupling and prevent propagation of faults across specific layers resulting in a preferable horizontal propagation of faults to the detriment of their vertical growth.

d) The significant distribution of the shallow faults in the uppermost part of the Nankai accretionary prism accommodates a significant part of the bending and stretching strain occurring during thrust-anticlines development, and subsequent local stress distribution and accommodation of strain during seismic events offshore Nankai.

Acknowledgements

Petroleum Technology Development Fund (PTDF), Nigeria (Ref: PTDF/ ED/PHD/MA/1328/18) was greatly acknowledged and thanked for funding the research study. This research used samples and data provided by the Integrated Ocean Drilling Program (IODP). We acknowledge Schlumberger for the provision of Petrel® software for seismic interpretation. We thank the reviewers and editor for their constructive comments, which greatly improved an early version of this manuscript.

References

Alves, T.M., Strasser. M., Moore, G. F., 2014. Erosional features as indicators of thrust fault activity (Nankai Trough, Japan). Mar. Geol. 356, 5–18.

Azevêdo, M. C., Alves, T.M., Fonseca, P.E., Moore, G.F., 2018. Strike-slip deformation reflects complex partitioning of strain in the Nankai Accretionary Prism (SE Japan). Tectonophysics 723 (2018) 81–94.

Bahroudi, A., Koyi, H.A., Talbot, C.J. 2003. Effect of ductile and frictional décollements on style of extension. Journal of Structural Geology, 25, 1401–1423.

Baudon, C., Cartwright, J., 2008. The kinematics of reactivation of normal faults using high resolution throw mapping. J. Struct. Geol. 30, 1072–1084.

Bird, P., 2003. An updated digital model of plate boundaries. Geochemistry Geophysics Geosystems, 4(3), 1027.

Cartwright, J., James, D., Bolton, Al, 2003. The genesis of polygonal fault system: a review. Geol. Soc. Lond. Spec. Publ. 216, 223–243.

Chang, C., Song, I., 2016. Present-day stress states underneath the Kumano basin to 2 km below Sea floor based on borehole wall failures at IODP site C0002, Nankai accretionary wedge. Geochem. Geophys. Geosyst. 17. http://dx.doi.org/10.1002/ 2016GC006562.

Childs, C., Nicol, A., Walsh, J.J., Watterson, J., 1996. Growth of vertically segmented normal faults. J. Struct. Geol. 18, 1389-1397.

Childs, C., Manzocchi, T., Walsh, J.J., Bonson, C.G., Nicol, A., Schöpfer, M.P.J. 2009. A geometric model of fault zone and fault rock thickness variations. Journal of Structural Geology, 31, 117–127.

Dahlstrom, C.D. A., 1969. Balanced cross sections. Can. J. Earth Sci. 6, 743-757.

Dahlen, F.A., Suppe, J., Davis, D., 1984. Mechanics of fold-and-thrust belts and accretionary wedges: cohesive Coulomb theory. J. Geophys. Res. Solid Earth 89 (B12), 10087–10101.

Davis, D., Suppe, J., Dahlen, F.A., 1983. Mechanics of fold-and-thrust belts and accretionary wedges. J. Geophys. Res. Solid Earth 88 (B2), 1153–1172.

DeMets, C., Gordon, R. G., Argus, D. F., 2010. Geologically current plate motions, Geophys. J. Int., 181, 1–80.

Expedition 316 Scientists, 2009. Expedition 316 Site C0006. In: Kinoshita, M., Tobin, H., Ashi, J., Kimura, G., Lallemant, S., Screaton, E.J., Curewitz, D., Masago, H., Moe, K.T. (Eds.), The Expedition 314/315/316 Scientists, Proc. IODP, 314/315/316, http://dx. doi.org/10.2204/iodp.proc.314315316.134.2009.
http://dx.doi.org/10.2204/iodp.proc.314315316.136.2009.

Expedition 333 Scientists, 2012. Site C0018. In: Henry, P., Kanamatsu, T., Moe, K. (Eds.), The Expedition 333 Scientists, Proc. IODP, 333. Integrated Ocean Drilling Program Management International, Inc., Tokyo. http://dx.doi.org/10.2204/iodp.proc.333. 103.2012.

Ferrill, D.A., Morris, A.P., 2003. Dilational normal faults. Journal of Structural Geology. 25, 183-196.

Ferrill, D.A., Morris, A.P., McGinnis, R.N., 2012. Extensional fault-propagation folding in mechanically layered rocks: the case against the frictional drag mechanism. Tectonophysics 576-577, 78-85.

Ferrill, D.A., Morris, A.P., 2008. Fault zone deformation controlled by carbonate mechanical stratigraphy, Balcones fault system, Texas. AAPG Bull. 92, 359-380.

Ferrill, D.A., McGinnis, R.N., Morris, A.P., Smart, K.J., Sickmann, Z.T., Bentz, M., Lehrmann, D., Evans, M.A., 2014. Control of mechanical stratigraphy on bed restricted jointing and normal faulting: eagle Ford Formation, south-central Texas, U.S.A. AAPG Bull. 98, 2477-2506.

Ferrill, D.A., McGinnis, R.N., Morris, A.P., McGinnis, R.N., Smart, K.J., Wigginton, S. S., Hill, N.J., 2017. Mechanical stratigraphy and normal faulting. Review article. J. Struct. Geol. 94, 275-302.

Ford, M., Williams, E.A., Artoni, A., Verg_es, J., Hardy, S., 1997. Progressive evolution of a fault-related fold pair from growth strata geometries, Sant Llorenç de Morunys, SE Pyrenees. J. Struct. Geol. 19, 413-441.

Gabrielsen, R.H., Sokoutis, D., Willingshofer, E., Faleide, J.I. 2016. Fault linkage across weak layers during extension: an experimental approach with reference to the Hoop Fault Complex of the SW Barents Sea. Petroleum Geoscience, 22, 123–135.

Hardy, S., Poblet, J., 2005. A method for relating fault geometry, slip rate and uplift data above fault-propagation folds. Basin Res. 17, 417-424.

Harris, R. A. 1998. Stress Triggers, Stress Shadows, and Implications for Seismic Hazard, Introduction to the Special Issue, J. Geophys. Res., 103, 24347-24358.

Ide, S., Baltay, A., Beroza, G.C., 2011. Shallow Dynamic Overshoot and Energetic Deep Rupture in the 2011 Mw 9.0 Tohoku-Oki Earthquake. Science, 332(6036), 1426-1429.

Jolly, B.A., Lonergan, L., Whittaker, A.C., 2016. Growth history of fault-related folds and interaction with seabed channels in the toe-thrust region of the deep-water Niger delta. Marine and Petroleum Geology 70 (2016) 58-76.

Kamei, R., Pratt, R.G., Tsuji, T., 2012. Waveform tomography imaging of a megasplay fault system in the seismogenic Nankai subduction zone. Earth Planet. Sci. Lett. 317, 343–353.

Kimura, G., Moore, G.F., Strasser, M., Screaton, E., Curewitz, D., Streiff, C., Tobin, H., 2011. Spatial and temporal evolution of the megasplay fault in the Nankai Trough. Geochem. Geophys. Geosyst. 12 (3).

Kimura, G., Koge, H., and Tsuji, T, 2018. Punctuated growth of an accretionary prism and the onset of a seismogenic megathrust in the Nankai Trough. Progress in Earth and Planetary Science, 5(1), 78.

Kinoshita, M. H., Tobin, N., Eguchi, S. N., 2010. Integrated Ocean Drilling Program Expedition 326 Scientific Prospectus, doi:10.2204/iodp.sp.326.2010.

Kopf, A, M., Strasser, N., Monsees, M. B., Underwood, J. G., 2010. Data report: Particle size analysis of sediments recovered during IODP Expeditions 315 and 316, Sites C0001–C0008, Nankai Trough forearc, off Japan, in Proceedings of the IODP, vol. 314/315/316, edited by M. Kinoshita et al., Integr. Ocean Drill. Prog. Manage. Int., Inc., Washington, D. C., doi: 10.2204/iodp.proc.314315316.207.2011.

Lackey, J, K., Regalla, C. A., and Moore, G, F., 2020. Tectonic influences on trench slope basin development via structural restoration along the outer Nankai accretionary prism, southwest Japan. Geochemistry, Geophysics, Geosystems, 21, 2020 GC009038. https://doi.org/ 10.1029/2020GC009038

Laubach, S.E., Olson, J.E., Gross, M.R., 2009. Mechanical stratigraphy and fracture stratigraphy. AAPG Bull. 93, 1413-1426.

Lee, S.J., Huang, B.S., Ando, M., Chiu, H.C., Wang. J.H., 2011. Evidence of large-scale repeating slip during the 2011 Tohoku-Oki earthquake, *Geophys. Res. Lett.*, 38, L19306.

Lewis, J.C., Byrne, T.B., Kanagawa, K., 2013. Evidence for mechanical decoupling of the upper plate at the Nankai subduction zone: constraints from core-scale faults at NantroSEIZE Sites C0001 and C0002. Geochem. Geophys. Geosyst. 14 (3), 620–633.

Lewis, K.B., Carter, L., Davey, F.J., 1994. The opening of Cook Strait: interglacial tidal scour and aligning basins at a subduction to transform plate edge. Marine Geology 116, 293–312.

Libak, A., Torabi, A., Alae, B., 2019. Normal fault geometric attribute variations with lithology: examples from the Norwegian Barents Sea. Geological Society London Special Publications, 495, DOI: 10.1144/SP495-2018-164.

Lin, W., Byrne, T.B., Kinoshita, M., McNeill, L.C., Chang, C., Lewis, J.C., Yamamoto, Y., Saffer, D.M., Casey Moore, J., Wu, H.-Y., Tsuji, T., Yamada, Y., Conin, M., Saito, S., Ito, T., Tobin, H.J., Kimura, G., Kanagawa, K., Ashi, J., Underwood, M.B., Kanamatsu, T., 2015. Distribution of stress state in the Nankai subduction zone, southwest Japan, and a comparison with Japan Trench. Tectonophysics 692, 120–130.

Lonergan, L., Cartwright, J.A., Jolly, R., 1998. 3-D geometry of polygonal fault systems. J. Struct. Geol. 20, 529–548.

Maunde, A., Alves, T.M., 2020. Impact of tectonic rafts' gravitational instability on fault reactivation and geometry. J. Struct. Geol. 130 (2020) 103916.

Micallef, A., Mountjoy, J.J., 2011. A topographic signature of a hydrodynamic origin for submarine gullies. Geology 39, 115–118.

Miyazaki, S., Heki, S., 2001. Crustal velocity field of southwest Japan: Subduction and arc-arc collision, J. Geophys. Res., 106, 4305–4326.

Moore, G. F., Bangs, N. L., Taira, A., Kuramoto, S., Pangborn, E., and Tobin, H. J., 2007. Three-dimensional splay fault geometry and implications for tsunami generation. Science, 318(5853), 1128–1131.

Moore, G. F., Boston, B. B., Sacks, A. F., Saffer, D. M., 2013. Analysis of normal fault populations in the Kumano Forearc Basin, Nankai Trough, Japan: 1. Multiple orientations and generations of faults from 3-D coherency mapping, Geochem. Geophys. Geosyst., 114, 1989–2002.

Moore, G.F., Park, J.O., Bangs, N.L., Gulick, S.P., Tobin, H.J., Nakamura, Y., Sato, S., Tsuji, T.,Yoro, T., Tanaka, H., Uraki, S., Kido, Y., Sanada, Y., Kuramoto, S., Taira, A., 2009. Structural and seismic stratigraphic framework of the NanTroSEIZE Stage 1 transect. In: Kinoshita, M., Tobin, H., Ashi, J., Kimura, G., Lallemant, S., Screaton, E.J., Curewitz, D., Masago, H., Moe, K.T., the Expedition 314/315/316 Scientists (Eds.), Proc. IODP, 314/315/316. (Integrated Ocean Drilling Program Management International, Inc.), Washington, DC. http://dx.doi.org/10.2204/iodp.proc. 314315316.102.2009.

Moore, G.F., Boston, B.B., Strasser, M., Underwood, M.B., Ratliff, R.A., 2015. Evolution of tectono-sedimentary systems in the Kumano Basin, Nankai trough forearc. Mar. Pet. Geol. 67, 604–616.

Mountjoy, J.J., Barnes, P.M., Pettinga, J.R., 2009. Morphostructure and evolution of submarine canyons across an active margin: Cook Strait sector of the Hikurangi Margin, New Zealand. Marine Geology 260, 45–68.

Park, J.O., Fujie, G., Wijerathne, L., Hori, T., Kodaira, S., Fukao, Y., Moore, G.F., Bangs, N.L., Kuramoto, S., Taira, A., 2010. A low-velocity zone with weak reflectivity along the Nankai subduction zone. Geology 38 (3), 283–286.

Pascoe, R., Hooper, R., Storhaug, K., Harper, H., 1999. Evolution of extensional styles at the southern termination of the Nordland Ridge, Mid-Norway: a response to variations in coupling above Triassic salt. In: Fleet, A.J., Boldy, S.A.R. (eds) Petroleum Geology of Northwest Europe: Proceedings of the 5th Conference. Geological Society, London, 83–90.

Peacock, D.C.P., Sanderson, D.J., 1991. Displacements, segment linkage and relay ramps in Normal fault zones. J. Struct. Geol. 13, 721–733.

Poblet, J., Hardy, S., 1995. Reverse modelling of detachment folds; application to the Pico del Aguila anticline in the South-Central Pyrenees (Spain). J. Struct. Geol. 17, 1707-1724.

Price, N. J., Cosgrove, J. W. 1990. Analysis of Geological Structures. Cambridge University Press, Cambridge

Ramsay, J. G. 1967. The Folding and Fracturing of Rocks. McGraw-Hill, New York.

Richardson, N.J., Underhill, J.R., Lewis, G., 2005. The role of evaporite mobility in modifying subsidence patterns during normal fault growth and linkage, Halten Terrace, Mid-Norway. Basin Research, 17, 203–223.

Shaw, J.H., Novoa, E., Connors, C.D., 2004. Structural controls on growth stratigraphy in contractional fault-related folds. In: McClay, K.R. (Ed.), Thrust Tectonics and Hydrocarbon Systems: AAPG Memoir, Vol. 82, pp. 400-412.

Shaw, J.H., Connors, C.D., Suppe, J., 2006. Seismic interpretation of contractional fault-related folds: an AAPG seismic atlas. AAPG Stud. Geol. 53, 156.

Smart, K.J., Ferrill, D.A., Morris, A.P., Bichon, B.J., Riha, D.S., Huyse, L., 2010. Geomechanical modeling of an extensional fault-propagation fold: Big Brushy Canyon monocline, Sierra del Carmen, Texas. AAPG Bull. 94, 221-240.

Strasser, M., Dugan, B., Kanagawa, K., Moore, G.F., Toczko, S., Maeda, L., The Expedition 338 Scientists, 2014. Site C0018: Proceedings of the Integrated Ocean Drilling Program. vol. 338. pp. 2.

Taira, A., 2001. Tectonic evolution of the Japanese Island Arc System. Annual Reviews of Earth and Planetary Science, 29(1), 109–134.

Tao, Z., Alves, T.M., 2019. Impacts of data sampling on the interpretation of normal fault propagation and segment linkage. Tectonophysics 762, 79-96.

Tsuji, T., Ashi, J., Ikeda, Y., 2014. Strike-slip motion of a mega-splay fault system in the Nankai oblique subduction zone. Earth, Planets Space 66 (1), 1–14.

Tvedt, A.B.M., Rotevatn, A., Jackson, C.A.L., Fossen, H., Gawthorpe, R.L. 2013. Growth of normal faults in multilayer sequences: A 3D seismic case study from the Egersund Basin, Norwegian North Sea. Journal of Structural Geology, 55, 1–20.

Van Tuyl, J., Alves, T.M., Moore, G.F., 2015. Strain decoupling reveals variable seismogenic risk in SE Japan (Nankai Trough). Geochem. Geophys. Geosyst. 16 (7), 2025–2037.

Wang, K., Hu, Y., 2006. Accretionary prisms in subduction earthquake cycles: The theory of dynamic Coulomb wedge. J. Geophys. Res. Solid Earth 111 (B6).

Welch, M.J., Davies, R.K., Knipe, R.J., Tueckmantel, C., 2009. A dynamic model for fault nucleation and propagation in a mechanically layered section. Tectonophysics 474, 473-492.

Withjack, M.O., Callaway, S., 2000. Active normal faulting beneath a salt layer: An experimental study of deformation patterns in the cover sequence. AAPG Bulletin, 84, 627–651.

Wu, H.Y., Chan, C.H., Kinoshita, M., Saito, S., 2013. Stress field observation and modelling from the NanTroSEIZE scientific drillings in the Nankai Trough system, SW Japan. Tectonophysics 600, 99–107.

Xiao, H., Suppe, J., 1989. Role of compaction in the listric shape of growth normal faults. AAPG Bull. 73, 777-786

Zoback, M.D., 2007. Reservoir Geomechanics. Cambridge University Press, Cambridge, 449 pp.

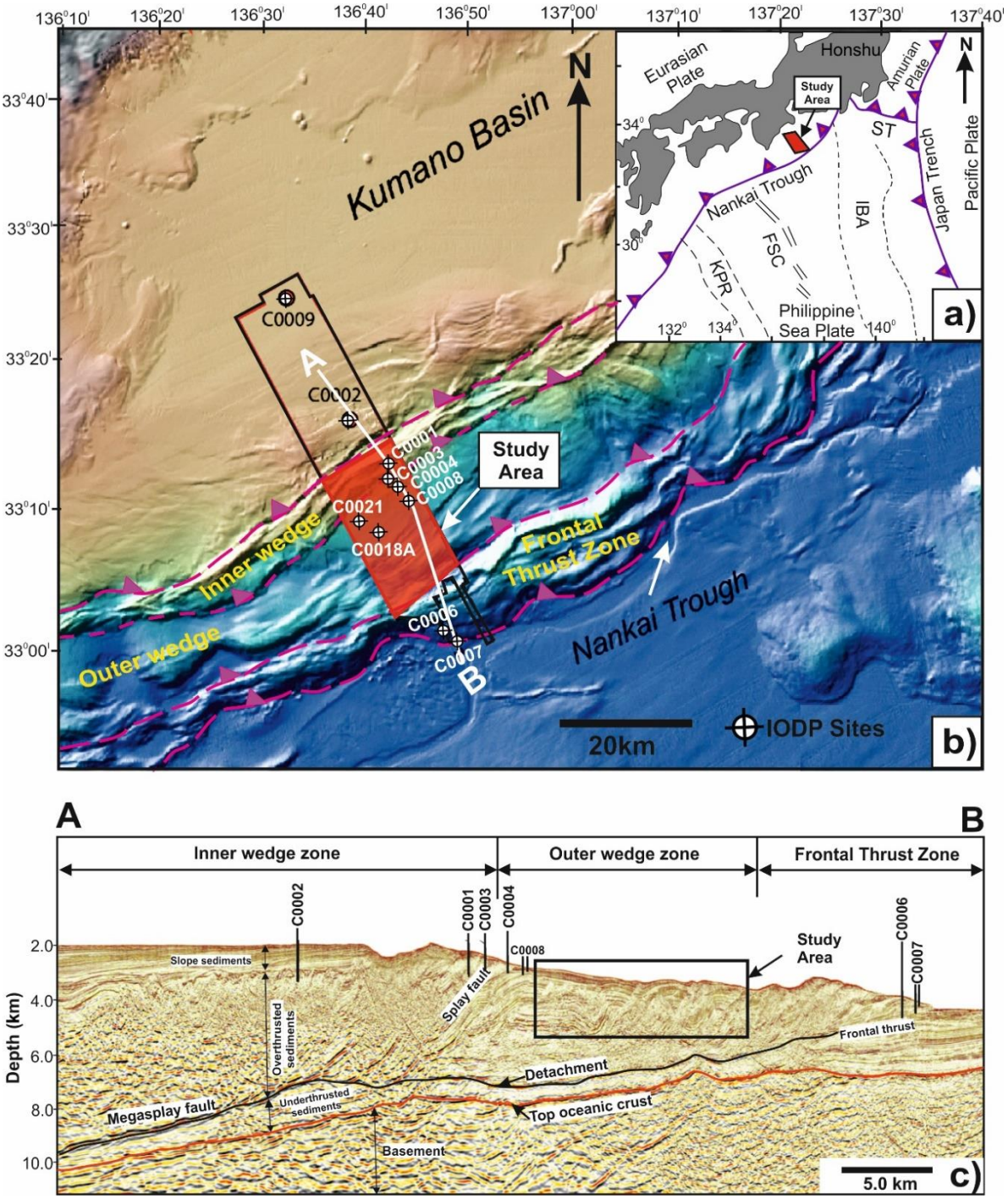

Fig. 1. a) Inset highlighting the three principal subduction trenches surrounding the Japanese Islands. i) the Nankai Trough, ii) the Sagami Trough (ST) and iii) the Japan Trench. The study area is shown by the red box. Figure modified from Bird (2003). b) Bathymetry map of the Kumano Basin and adjacent region to the Nankai accretionary prism highlighting structural zones, the location of IODP sites and the location of the study area (red box). Figure Modified from Moore et al. (2013). Where KPR-Kyushu-Palau Ridge; FSC –Fossil Spreading Centre; IBA-Izu-Bonin Arc; ST -Sagami Trough; OKP-Okhotsk Plate, MSFZ-Megasplay Fault Zone; IODP - Integrated Ocean Drilling Programme. c) Arbitrary line through the 3-D seismic volume along some of the drilled sites (Moore et al., 2009) highlighting structural zones and study area within the outer wedge zone.

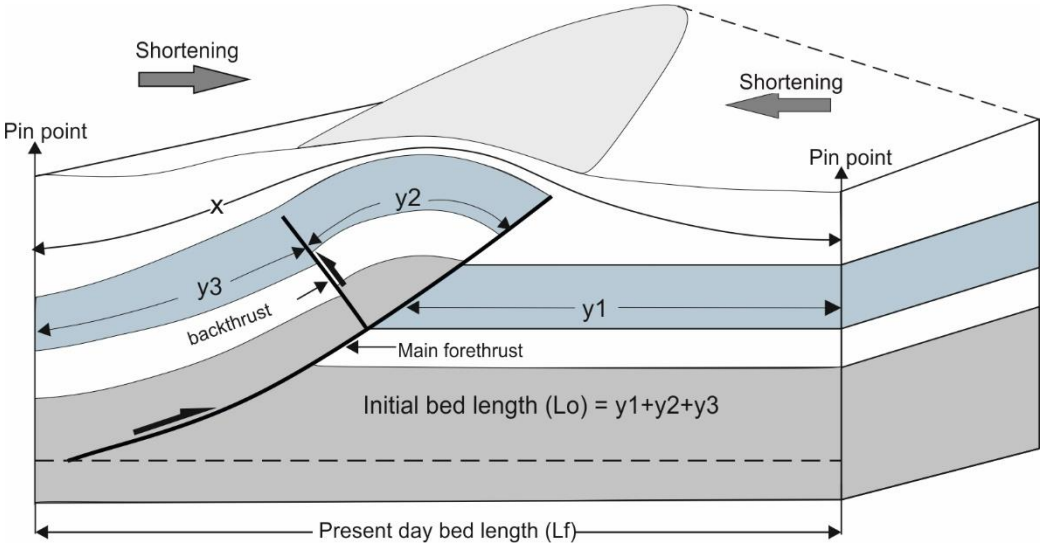

Fig. 2. Schematic section highlighting strain-distance (e-x) measurement through folded and faulted strata using line-length balancing techniques. Where initial bed length, Lo through thrusted strata is expressed as: Lo = y1+y2+y3, and through overlapping strata is: Lo = x. Lf is the present-day bed length after deformation.

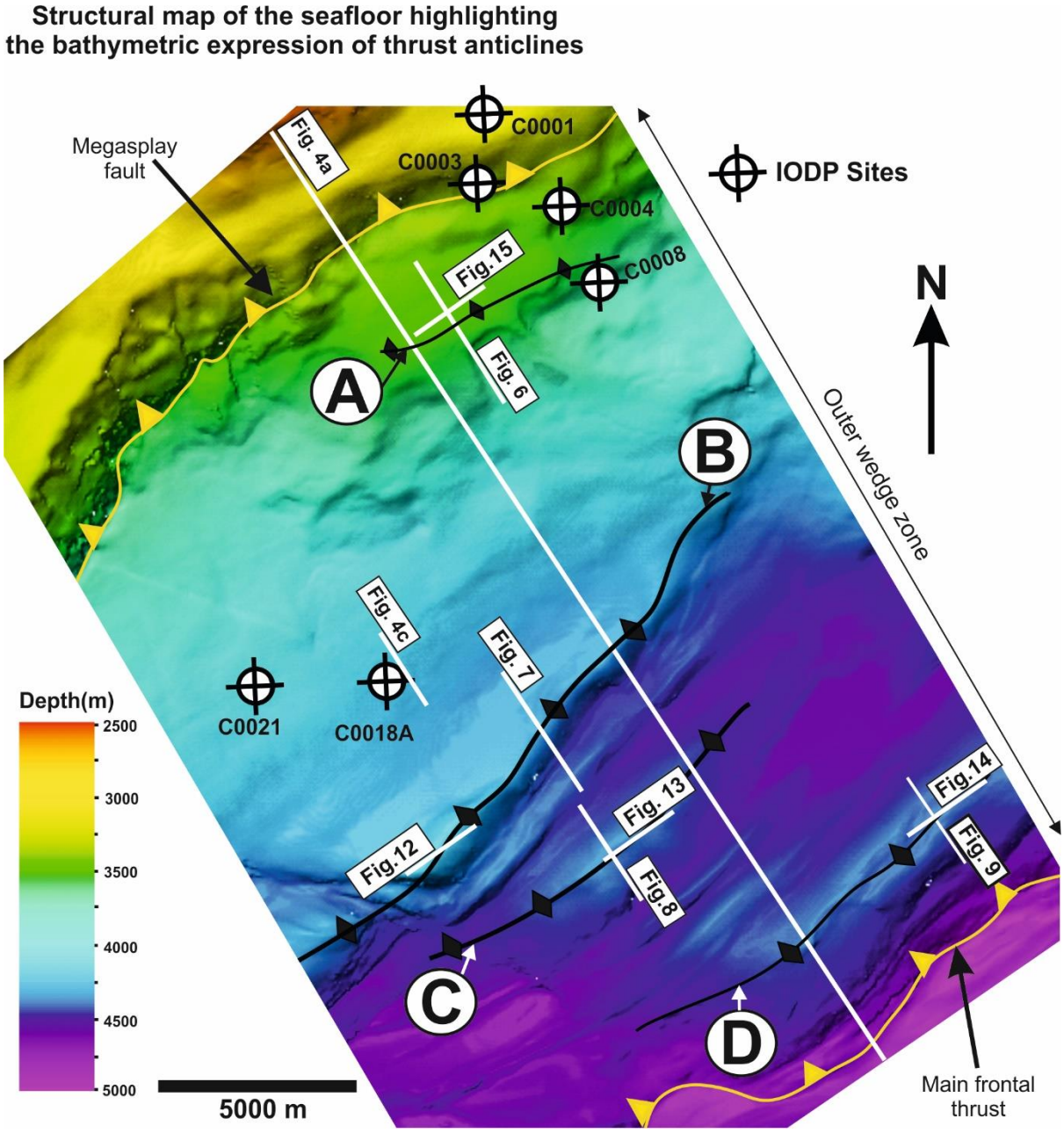

Fig. 3. Structural map of the seafloor highlighting the bathymetric expression of thrust anticlines, trending perpendicular to the regional bathymetric slope. Seismic profile lines and key Integrated Ocean Drilling Programme (IODP) Sites are shown on the map. Where A, B, C and D represent Thrust Anticlines A to D.

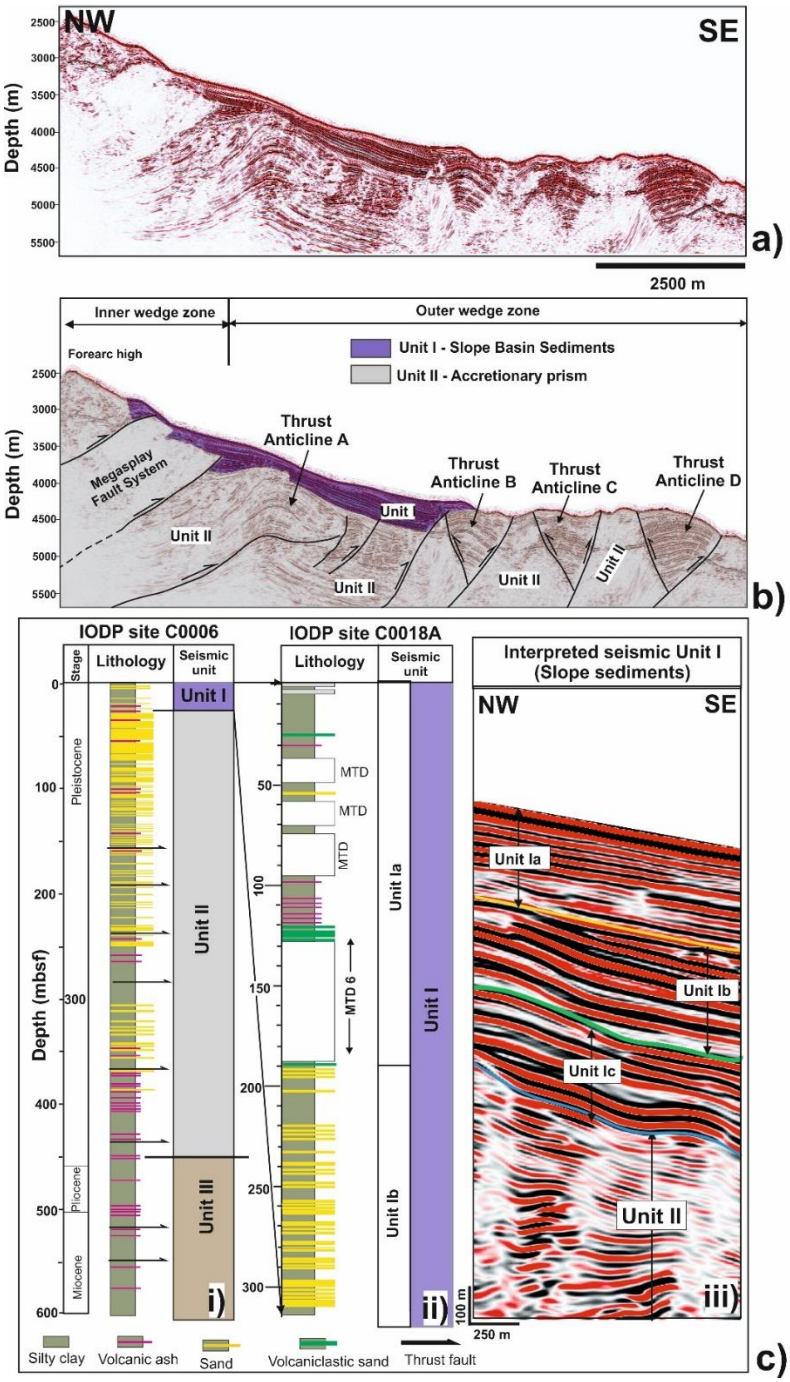

Fig. 4. a) Uninterpreted and b) interpreted seismic section across the deep-water Nankai accretionary prism highlighting the structural styles, interpreted seismic units (Units I and II) and the four Thrust Anticlines A to D studied in this work. c) Seismic-stratigraphic correlation amongst the interpreted seismic units, stratigraphic ages and lithologies in the Nankai accretionary prism, SE Japan. Unit I represent relatively undeformed slope sediments (Expedition 333 Scientist 2012; Kimura et al., 2011; Alves et al., 2013; Strasser et al., 2014). Unit II – overthrust sediments (Park et al., 2010). IODP well C0018A highlight the subdivision of Unit I into Units Ia, Ib and Ic based on Strasser et al. (2014) and Alves et al. (2013). IODP Site C0006 (Expedition 316 Scientists, 2009) which is ~ 4 km SE from the seismic profile (see Fig. 1c) was correlated with the seismic unit II interpreted in this work.

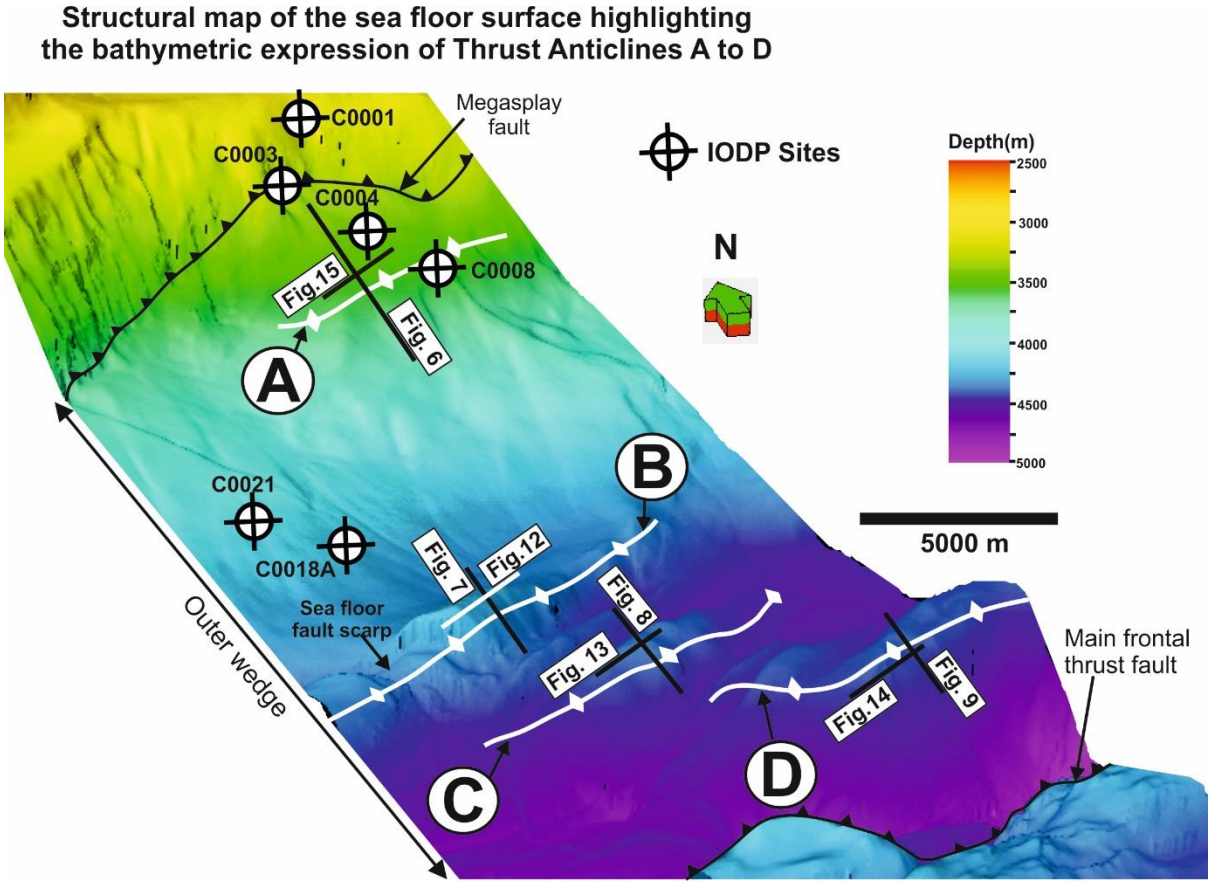

Fig. 5. 3D seafloor structural map of the study area highlighting bathymetric expression of the four studied thrust anticlines (A to D) with a linear NE-SW trend, perpendicular to the regional bathymetric slope. Thrust Anticlines B, C and D deformed the modern seafloor and develops a corresponding bathymetric high of up to 102 m, 113 m, and 182 m in relief, evident for active growth at present. Thrust Anticline B developed a seafloor fault scarp. Seismic profile lines and key Integrated Ocean Drilling Programme (IODP) Sites are shown on the map. Where A, B, C and D represent Thrust Anticlines A to D.

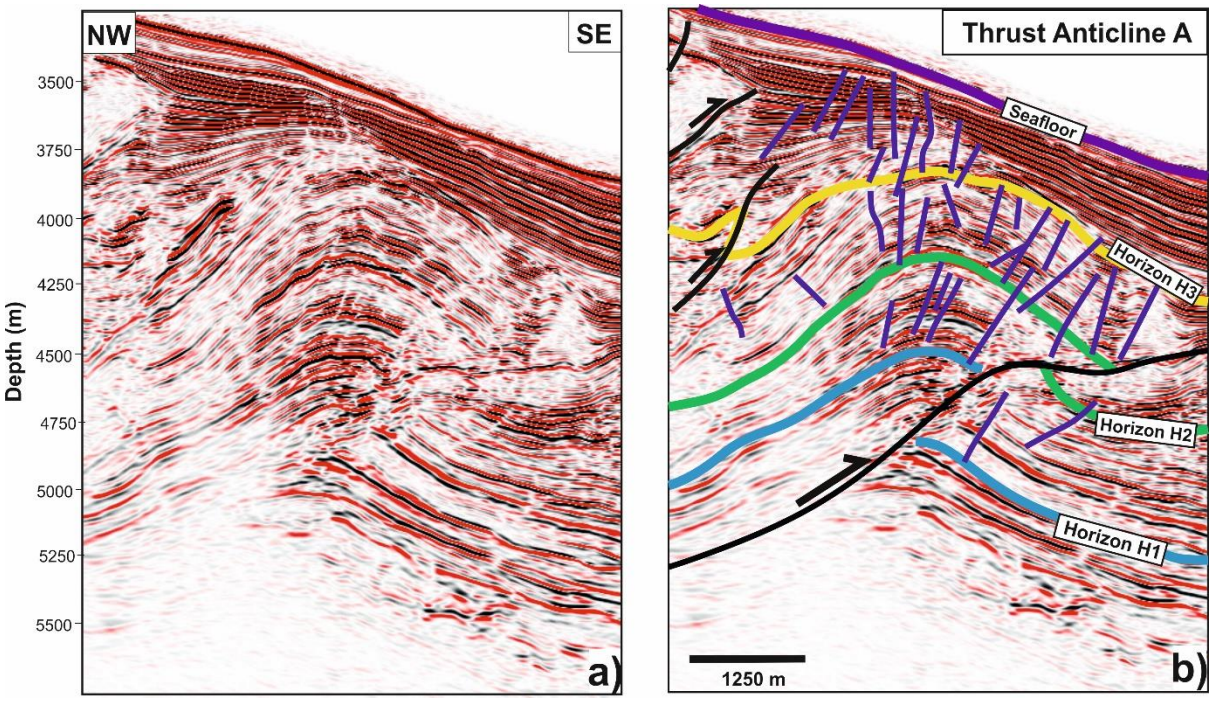

Fig. 6. Uninterpreted and interpreted seismic sections across the most landward Thrust Anticline A highlighting the interpreted horizons, shallow faults and major curved forethrust on the front limb and in the anticline core. The shallow faults are localised in the uppermost part of the accreted (Unit II) and slope (Unit I) sediments.

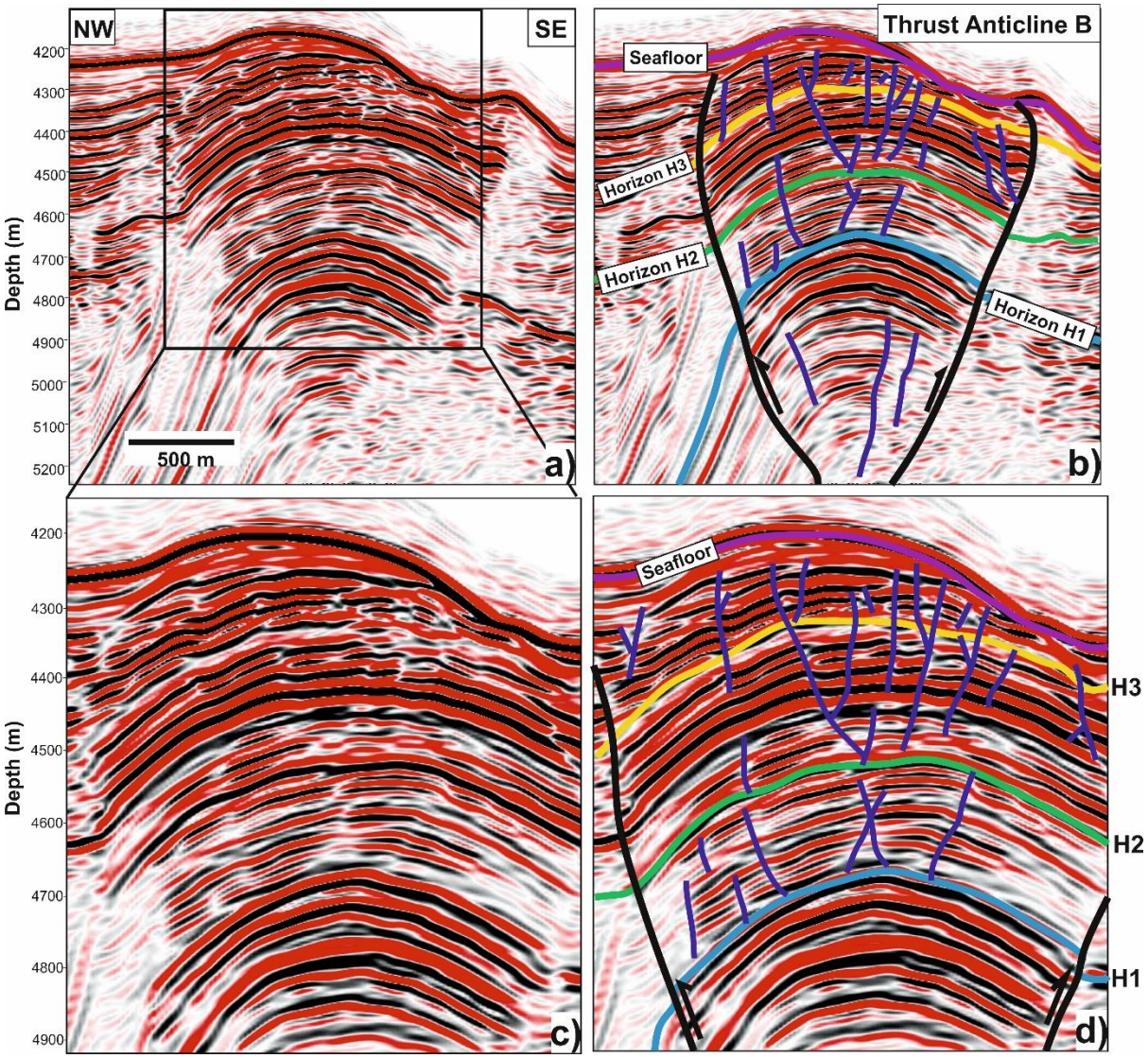

Fig. 7. Uninterpreted and interpreted seismic sections across Thrust Anticline B highlighting the geometry of major thrust and shallow fault populations. The shallow faults are localised within the hinge region of the thrust anticline. These faults are closely-spaced and vertically segmented, with some appear to propagate and link with other faults. Location shown in Figs. 3 and 5.

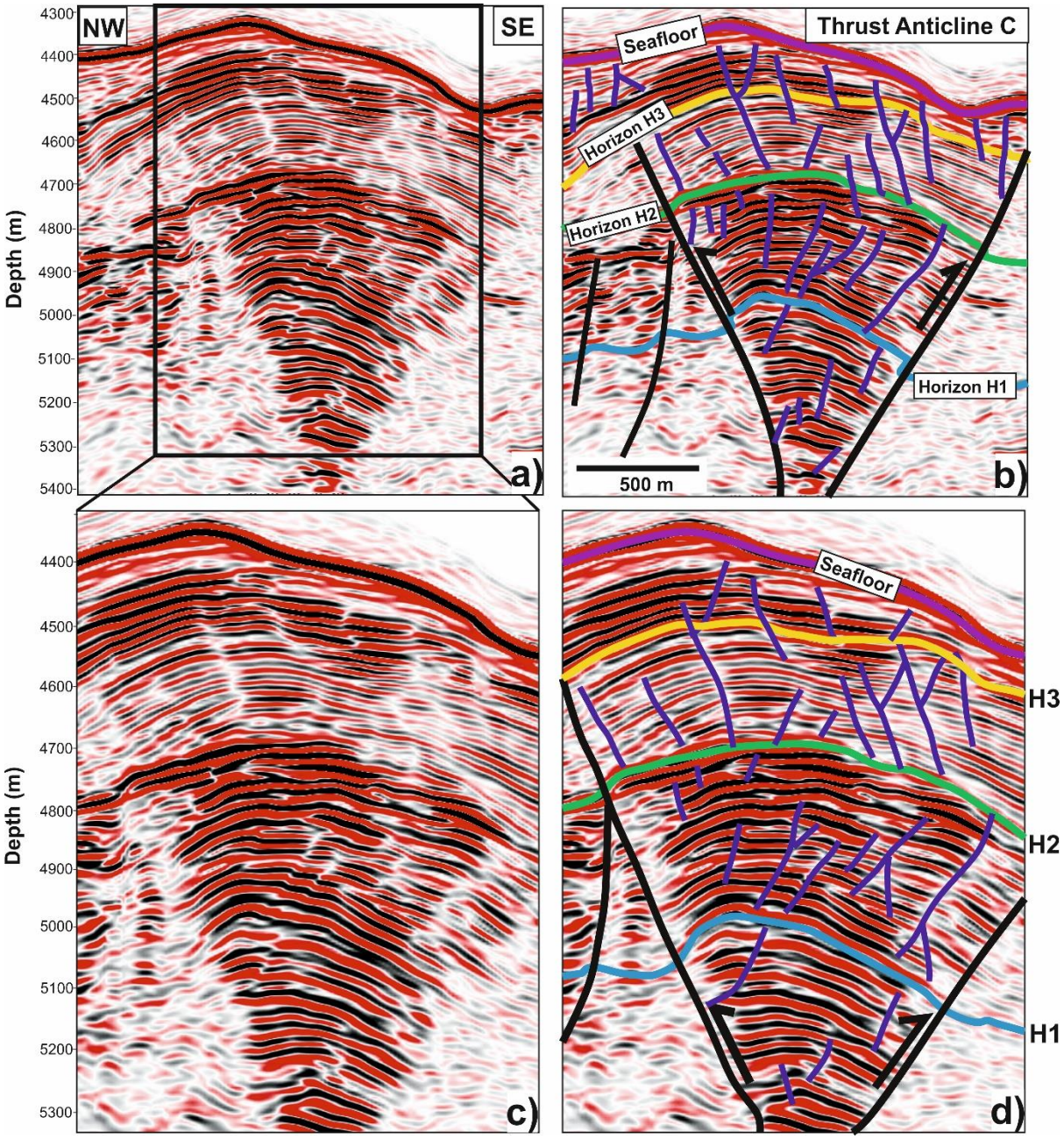

Fig. 8. Uninterpreted and interpreted seismic sections across Thrust Anticline C highlighting the interpreted horizons, major thrust faults, and shallow faults. The shallow faults are localised within the hinge region of the thrust anticline. These faults are vertically segmented and offset strata at shallow stratigraphic levels, with some appearing to propagate and link with other faults. Location shown in Figs. 3 and 5.

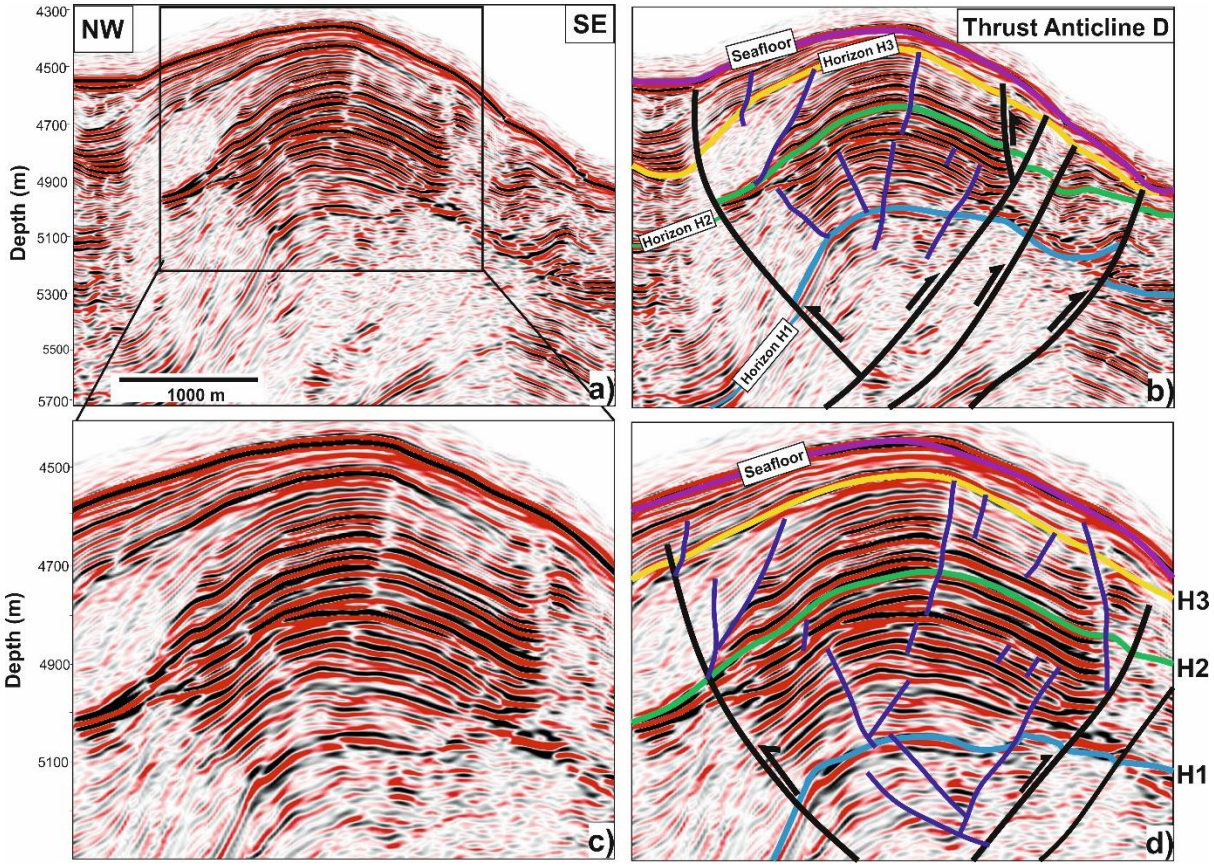

Fig. 9. Uninterpreted and interpreted seismic sections across the most seaward Thrust Anticline D highlighting the interpreted horizons, major thrust faults, and shallow faults. The shallow faults are localised in the uppermost part of the accreted sediments (Unit II), within the hinge region of the thrust anticline. These faults are closely-spaced and segmented, with some appear to propagate and link with other faults. Location shown in Figs. 3 and 5.

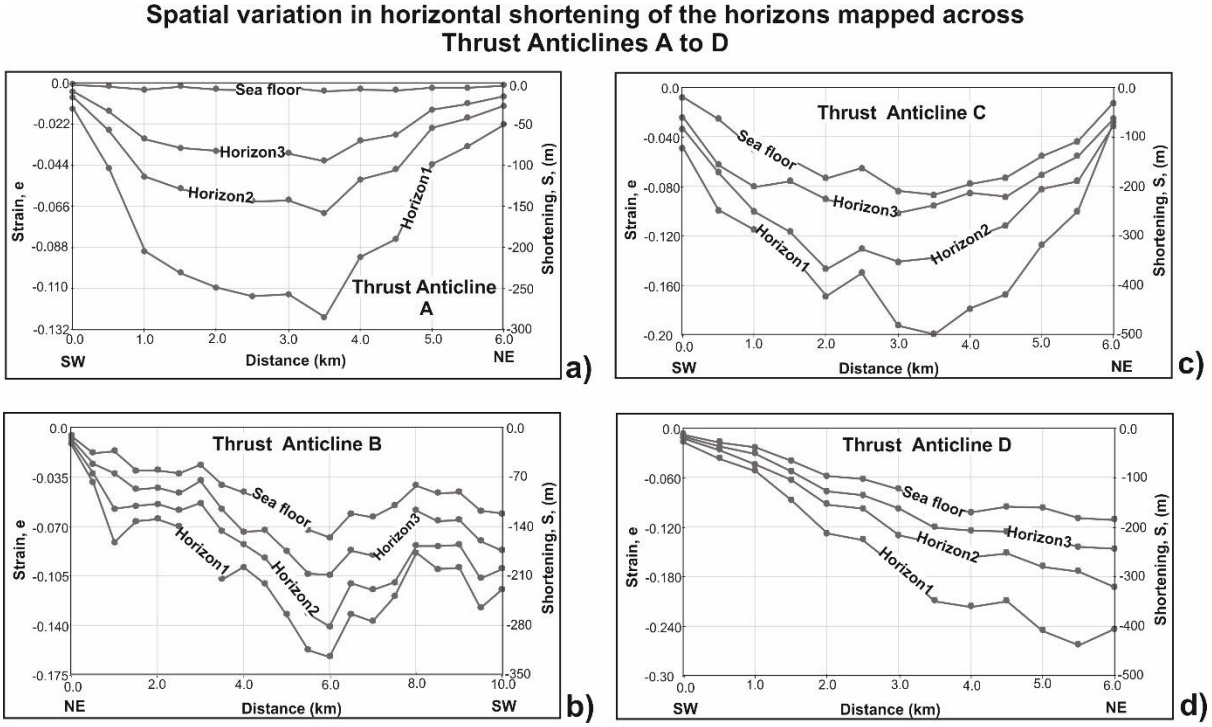

Fig. 10. Strain–distance (e-x) plots illustrating the along-strike variation in the thrust anticlines shortening for the mapped horizons. Strain distribution in the mapped horizons increases with depth (i.e. it is higher in the older horizons and lower in the younger horizons), reflecting growth of the structure through time.

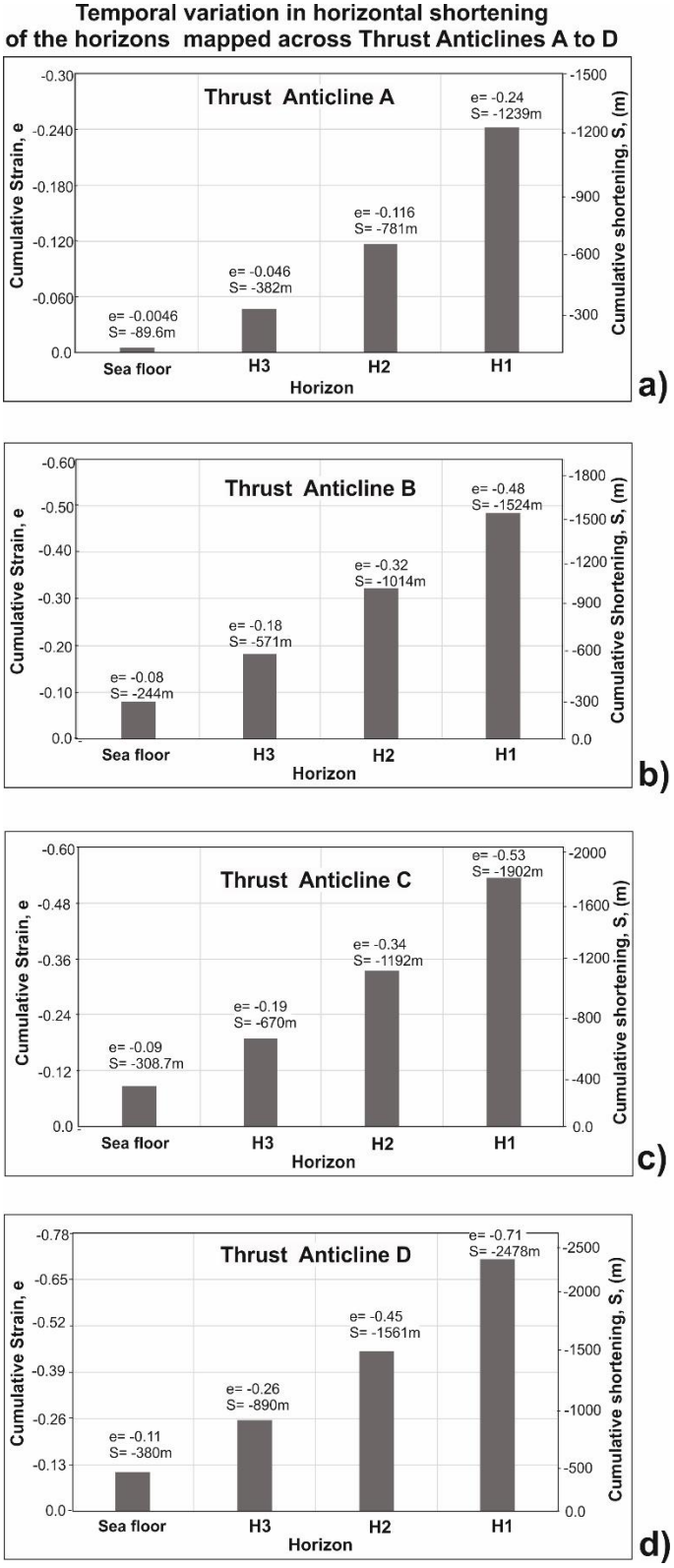

Fig. 11. Cumulative strain plots illustrating the variation in the thrust anticlines shortening for the mapped horizons. The maximum cumulative shortening recorded by the most landward Thrust Anticline A (1239 m), is approximately half of the maximum cumulative shortening recorded for the most seaward Thrust Anticline D (2478 m), indicating a trench-ward increase in horizontal shortening of the thrust anticlines.

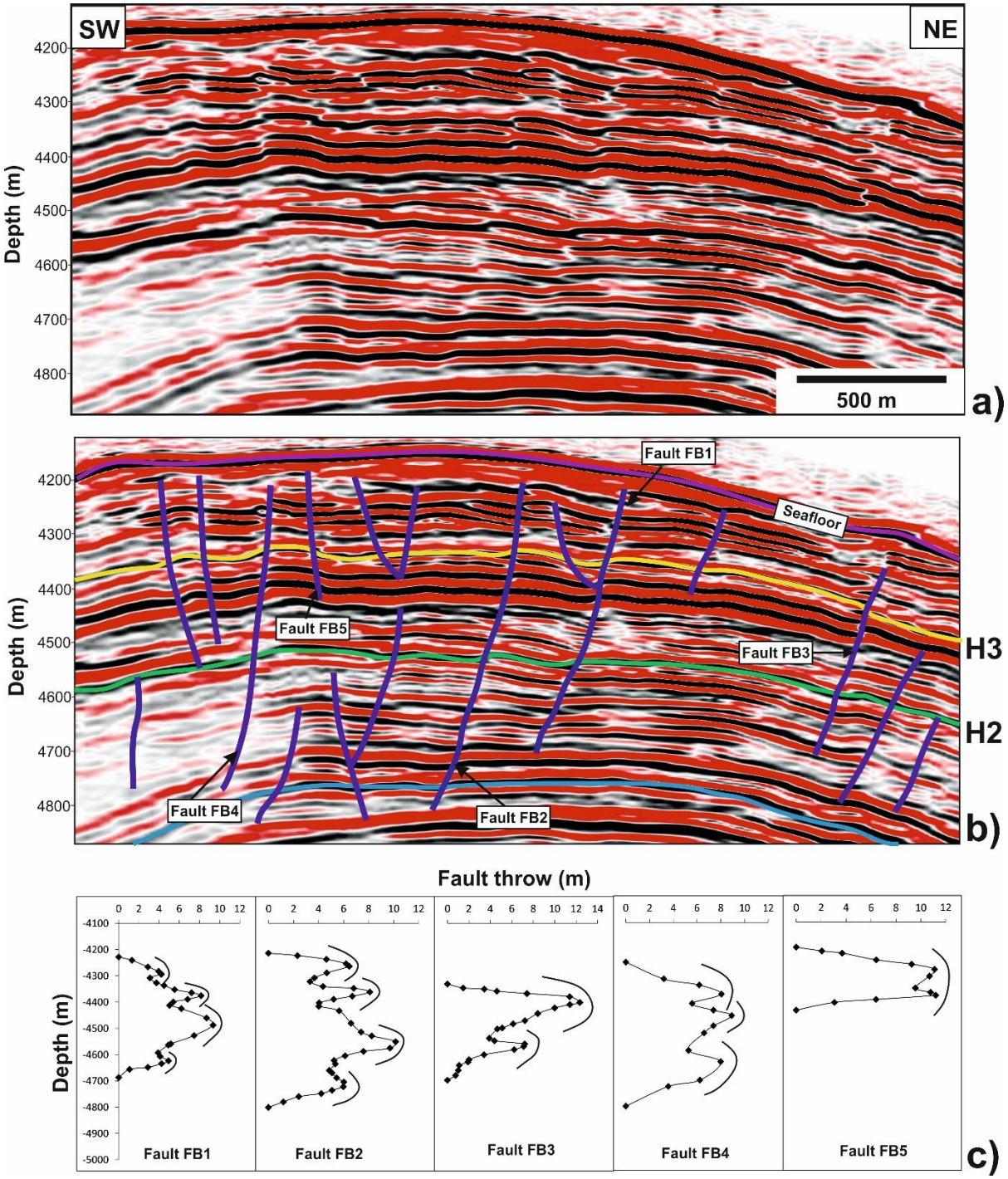

Fig. 12. a) Uninterpreted and b) interpreted seismic sections highlighting some of the features of shallow fault populations around the hinge region of the Thrust Anticline B. The faults are vertically segmented, with some appear to propagate and link with other faults, c) Representative vertical throw distribution of the shallow faults. Multiple throw maxima separated by throw minima on the throw distribution profiles show that fault segment linkage is a common process during the growth of shallow faults.

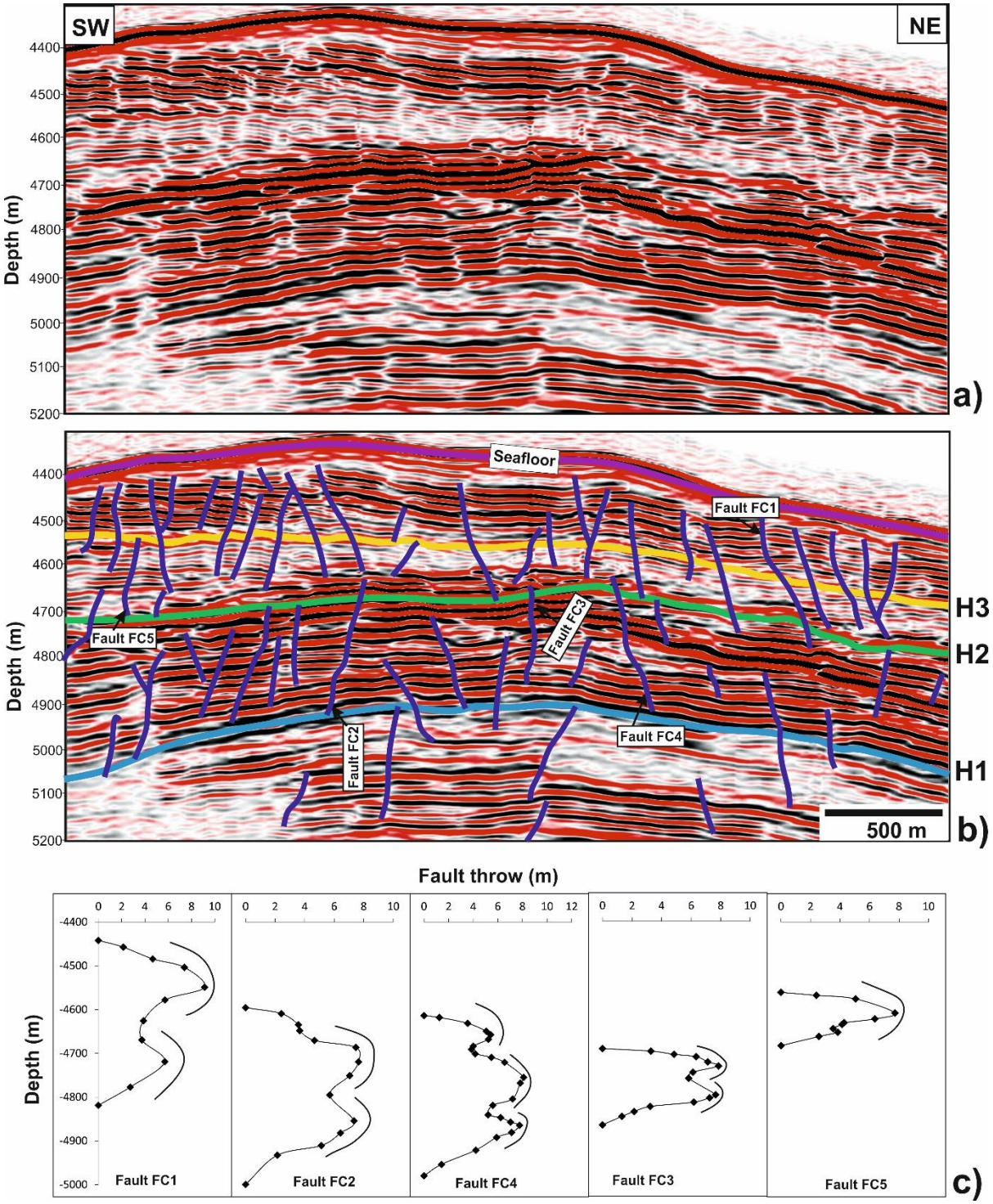

Fig. 13. a) Uninterpreted and b) interpreted seismic sections highlighting the geometry of shallow fault populations around the hinge region of the Thrust Anticline C. These faults are closely-spaced and vertically segmented, with some appear to propagate and link with other faults, c) Representative vertical throw distribution of the shallow faults. The faults are vertically segmented with relatively larger fault throw maxima. Fault segments with throw maxima nucleate first in more competent (strong) intervals and are later linked by throw minima in less competent (weak) intervals.

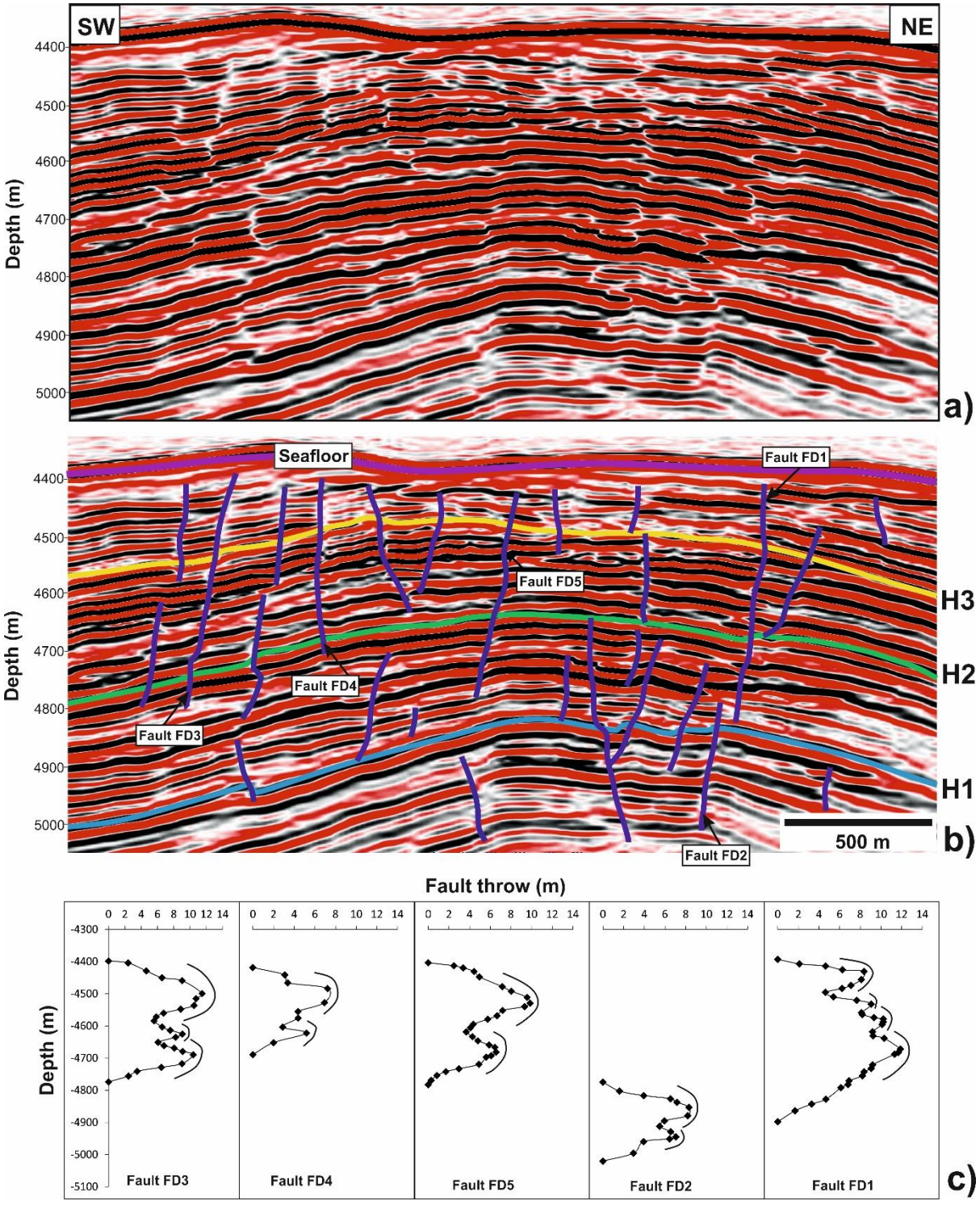

Fig. 14. a) Uninterpreted and b) interpreted seismic sections highlighting the geometry of shallow fault populations around the hinge region of the Thrust Anticline D. The faults are vertically segmented, with some appear to propagate and link with other faults, c) Representative vertical throw-depth (T–Z) profiles of the shallow faults. Fault segments with throw maxima nucleate first in more competent (strong) intervals and are later linked by throw minima in less competent (weak) intervals.

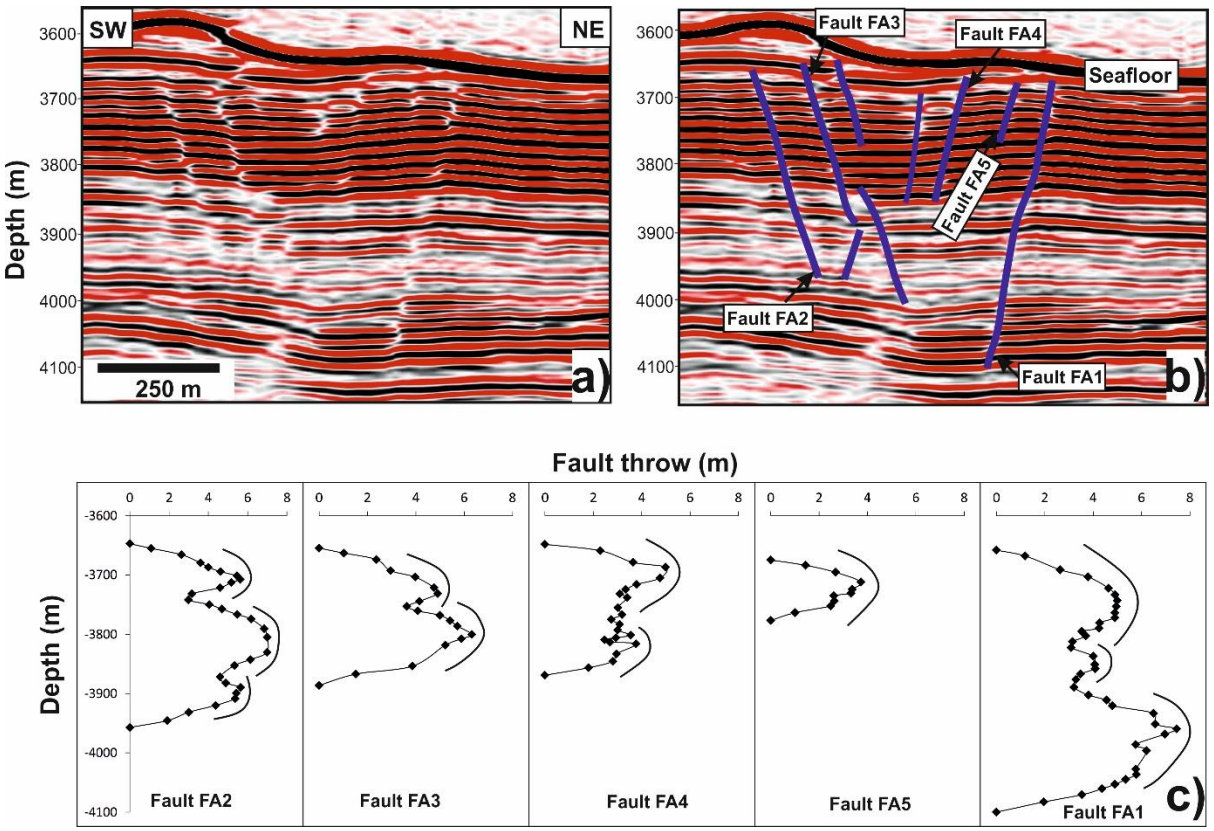

Fig. 15. a) Uninterpreted and b) interpreted seismic sections highlighting the typical geometry of shallow fault populations in the slope basin sediments (Unit I). These faults are segmented, with some appear to propagate and link with other faults, c) Representative vertical throw-depth (T–Z) profiles of the shallow faults. These profiles highlight fault propagating and growing by segment linkage, where two separate fault segments with throw maxima in more competent (strong) intervals have propagated towards each other and linked in less competent (weak) interval with throw minima.

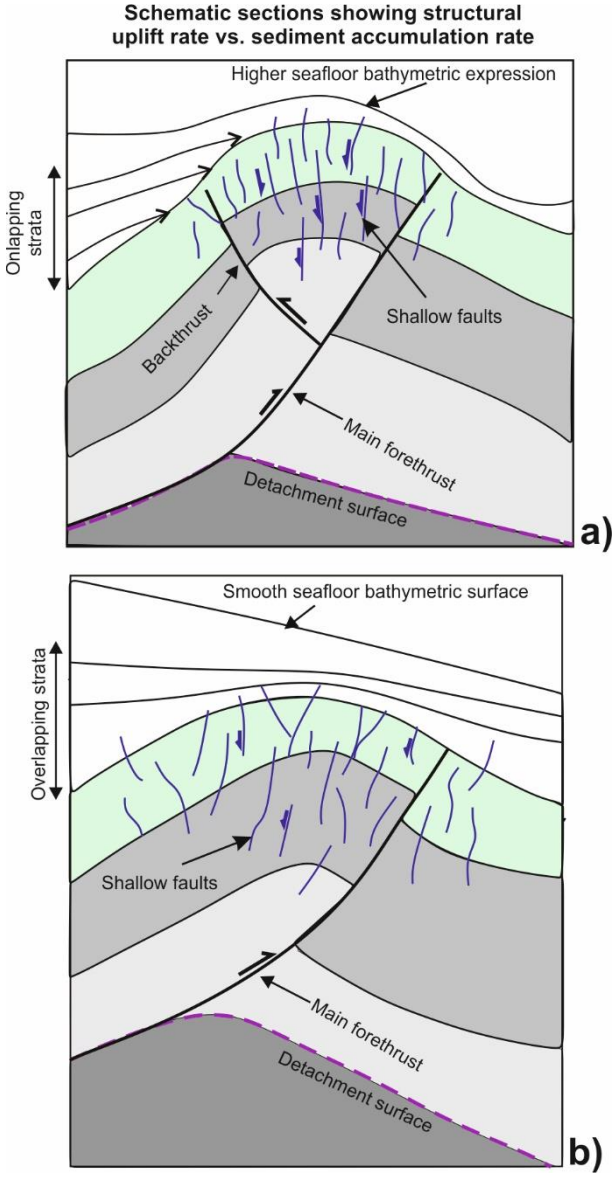

Fig. 16. Schematic sections depicting the relationship between structural uplift rate and sediment accumulation rate based on the interpreted seismic data. a) Higher uplift rate relative to sediment accumulation rate. Growth strata mainly onlap the growing structure, leading to development of seafloor bathymetric expression associated with the growing structure (e.g., Thrust Anticlines B, C and D). b) Higher sediment accumulation rate relative to uplift rate. Growth strata mainly overlap the growing structure, leading to a relatively smooth sea floor bathymetric expression (e.g., Thrust Anticlines A).

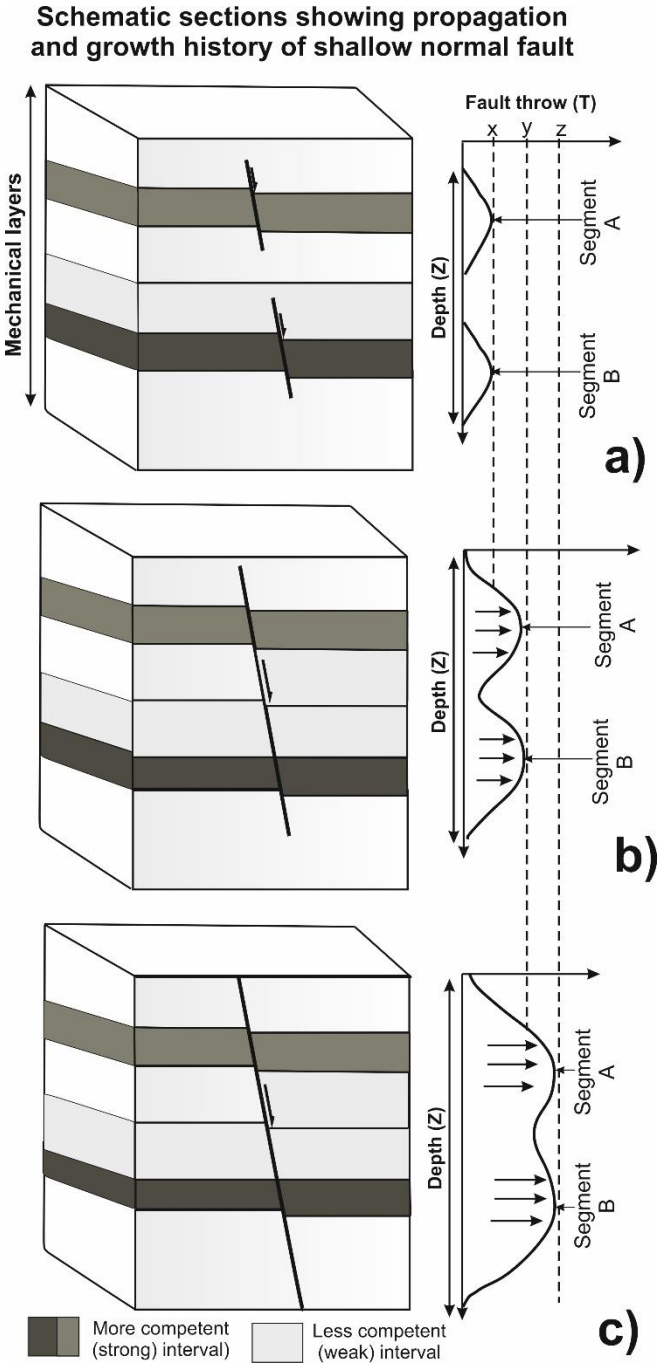

Fig. 17. Schematic sections illustrating the vertical growth of shallow faults by segment linkage. a) Faults nucleate first in more competent (strong) intervals with larger throw maxima, b) the nucleated faults propagate outwards into incompetent (weak) intervals. Incompetent (weak) intervals can prevent or slow faults from propagation across other layers, resulting in a preferable horizontal propagation of faults rather than the vertical growth. c) a shift in fault position across an incompetent layer can result in vertical fault segmentation, where the fault segments with throw maxima in more competent l(strong) intervals can be hard- or soft-linked by throw minima in less competent (weak) intervals.